Airway tissue stem cells reutilize the embryonic proliferation regulator, Tgfß-Id2 axis, for tissue regeneration

Hirofumi Kiyokawa[1], Akira Yamaoka[1], Chisa Matsuoka[1], Tomoko Tokuhara[2], Takaya Abe[2], Mitsuru Morimoto[1,*]

1 Laboratory for Lung Development and Regeneration, RIKEN Center for Biosystems Dynamics Research, Kobe 650-0047, Japan

2 Laboratory for Animal Resources and Genetic Engineering, RIKEN Center for Biosystems Dynamics Research, Kobe 650-0047, Japan

*Correspondence: mitsuru.morimoto@riken.jp

Summary

During development, quiescent basal stem cells are derived from proliferative primordial progenitors through the cell cycle slowdown. In contrast, quiescent basal cells contribute to tissue repair during adult tissue regeneration by shifting from slow-cycling to proliferating and subsequently back to slow-cycling. Although sustained basal cell proliferation results in tumorigenesis, the molecular mechanisms regulating these transitions remain unknown. Using temporal single-cell transcriptomics of developing murine airway progenitors and *in vivo* genetic validation experiments, we found that Tgfß signaling slowed down cell cycle by inhibiting *Id2* expression in airway progenitors and contributed to the specification of slow-cycling basal cell population during development. In adult tissue regeneration, reduced Tgfß signaling restored *Id2* expression and initiated epithelial regeneration. *Id2* overexpression and *Tgfbr2* knockout enhanced epithelial proliferation; however, persistent *Id2* expression in basal cells drove hyperplasia at a rate that resembled a precancerous state. Together, the Tgfß-Id2 axis commonly regulates the proliferation transitions in airway basal cells during development and regeneration, and its fine-tuning is critical for normal regeneration while avoiding basal cell hyperplasia.

Introduction

Tissue stem cells contribute to homeostasis through the strict regulation of cell proliferation (Leach and Morrisey, 2018; Yanger and Stanger, 2011). Under normal conditions, most of the tissue stem cells are maintained in the quiescent or slow-cycling state by suppression of cell cycle progression (Furutachi, et al., 2015; Desai, et al., 2014; Cheung and Rando, 2013). However, following injury, they undergo self-renewal by re-entering the cell cycle for tissue regeneration (Cheung and Rando, 2013; Yanger and Stanger, 2011). The precise regulation of the transitions of the stem cell population between the quiescent/slow-cycling and active cell cycle is essential for tissue homeostasis; the dysregulation of this transition is related to pathological disorders, such as cancer (Feitelson, et al., 2015; Lapouge, et al., 2011; Barker, et al., 2009). However, the molecular mechanism regulating the stem cells' transitions to the proliferation mode remains unknown. Thus, understanding such molecular mechanism is important for stem cell biology and human health.

Quiescent tissue stem cells are selected and segregated from the primordial progenitors during tissue development. It has been reported that the tissue stem cells of hair follicles and the brain enter the quiescent/slow-cycling state as they differentiate from the primordial progenitors during organogenesis (Furutachi, et al., 2015; Shyer, et al., 2015;

Gancz, et al., 2011; Nowak, et al., 2008; Mikkola and Orkin, 2006). These studies have demonstrated the importance of cell cycle slowdown for the specific quiescent tissue stem population at the early stage of tissue development. For example, in the development hair follicle stem cells, slow-cycling cells expressing stem cell markers appear in the primordial surface ectoderm. This population differentiates into mature quiescent hair follicle stem cells at the later stage. The ablation of this slow-cycling population compromised epidermal would repair due to the decreased number of tissue stem cells (Nowak, et al., 2008). Thus, cell cycle slowdown within primordial progenitors must be critical for the specification of tissue stem cell population during development. However, the molecular mechanism inducing the cell cycle attenuation in the progenitor population remains largely unknown.

Adult airway epithelium shows a low cellular turnover rate, usually more than 4 months, in rodents (Rock, et al., 2009; Blenkinsopp, 1967). It possesses a substantial ability to regenerate damaged cells in response to severe injuries caused by a viral infection or chemical toxicity (Hogan, et al., 2014; Kotton and Morrisey, 2014; Rock, et al., 2011). Airways display pseudostratified epithelium, which comprises four major cell types, including ciliated, club, neuroendocrine (NE), and basal cells (Herriges and Morrisey, 2014; Morrisey and Hogan, 2010). Airway basal cells are well-characterized epithelial

65 tissue stem cells (Pardo-Saganta, et al., 2015; Rock, et al., 2009; Hong, et al., 2004) whose
66 capacity for self-renewal is strictly regulated so that they remain as slow-cycling basal
67 cells for more than 16 weeks (Rock, et al., 2009). The dysregulation of airway basal cells
68 can result in fatal diseases, including squamous cell carcinoma (Lapouge, et al., 2011).
69 Sulfur dioxide (SO_2) inhalation-induced tissue injury is known as an experimental model
70 for airway epithelial injury-regeneration; in this model, slow-cycling basal cells can be
71 activated to proliferate and produce transit-amplifying cells within 48 hours. After these
72 proliferating transit-amplifying cells repair the epithelial damage, they subsequently start
73 differentiating into luminal cells to stop the cell cycle progression and hyperplasia (Pardo-
74 Saganta, et al., 2015; Rock, et al., 2011).

75 During airway development, the basal cells are selected and segregated from primordial
76 airway progenitors, which show high proliferation profile and arise from the ventral
77 foregut (Herriges and Morrisey, 2014; Morrisey and Hogan, 2010). During lung
78 development, primordial airway progenitors commit to the cell lineage, slowing down the
79 cell cycle and acquiring mature cells' canonical markers (Herriges and Morrisey, 2014).
80 We had previously reported the crucial function of Notch signaling in alternative cell fate
81 selection in club, ciliated, and NE cells (Kiyokawa and Morimoto, 2020; Arner, et al.,
82 2015; Consortium, et al., 2014; Morimoto, et al., 2012; Morimoto, et al., 2010). However,

the specific mechanism of slow-cycling basal progenitors during development remains unclear.

In the present study, to unveil the molecular mechanism that establishes slow-cycling basal cells, we delineated a comprehensive developmental roadmap of mouse airway epithelial cells using time series, single-cell transcriptome analyses. This approach and *in vivo* lineage tracing experiments defined the trajectory of basal cell differentiation and identified novel *Krt17*$^{+}$ basal progenitors. We also found that genes encoding inhibitors of DNA-binding/differentiation (Id) proteins promote epithelial proliferation. Tgfβ signaling reduces *Id2* expression to slow down the progenitors' cell cycle around E14.5, inducing the *Krt17*$^{+}$ basal progenitors and *Scgb3a2*$^{+}$ luminal progenitors.

In addition, we demonstrated that the Id2 dosage regulates the proliferation of mature basal cells. At the perinatal and adult stages, *Id2* expression is further restricted and maintained at low levels only in mature basal cells to ensure their proliferation potential. The SO_2-exposure mediated injury-regeneration model using adult mice showed that an increased *Id2* expression by Tgfβ suppression initiated the regeneration of the injured epithelia via promoting basal cells' re-entry into the cell cycle. Furthermore, the artificial enhancement of *Id2* expression boosted basal cell proliferation and resulted in basal cell hyperplasia, which resembles a precancerous state. These results imply that the fine-

101 tuning of *Id2* expression is critical for normal tissue regeneration while avoiding
102 tumorigenesis.

103 In summary, we demonstrate that the Tgfß-Id2 axis is a shared, critical regulator of the
104 transition between the active proliferation and slow-cycling mode in airway stem cells
105 during development and adult tissue regeneration.

106

107 **Results**

108 **Time series single-cell RNA sequencing (scRNA-seq) analyses to delineate a**
109 **developmental roadmap of airway epithelial cells, including basal cells**

110 We aimed to identify a high-fidelity marker of early basal progenitors to elucidate the
111 developmental process of mature basal cells; p63 is a well-known marker for basal cells
112 but is not restricted to basal progenitors at early development (Yang, et al., 2018). We
113 used a droplet-based scRNA-seq with approximately 3500 epithelial cells at six time
114 points from E12.5 to E18.5 (Figure 1A). This approach allowed us to delineate a
115 comprehensive lineage map of airway epithelial cells derived from respiratory endoderm
116 during embryogenesis. We visualized the distinct populations with cluster analysis using
117 the t-SNE algorithm. Uniform progenitors at E12.5 and E13.5 changed transcriptome

118 profiles at E14.5 and acquired cell type-specific gene signatures by E16.5 (Figures 1B
119 and S1B, also see Figure 3I). During E12.5 to E14.5, proliferative markers are frequently
120 detected and are the major determinants for cell clustering analysis (Figure 1B and see
121 Figure 3A). Epithelial progenitors eventually differentiated into three major populations,
122 basal, club, and ciliated cells, and one minor population, NE cells (Figure 1B). This
123 transcriptome clustering and the pseudo-time trajectory analysis using Monocle (Figure
124 1C) demonstrated that the lineage-specific transcriptional patterns were determined
125 between E14.5 and E16.5. *Foxj1*$^{+}$ ciliated cells first appeared at approximately E14.5,
126 which was suggested because some of the E14.5 progenitors were classified in the ciliated
127 cell population (Figure 1B). Other progenitors differentiated into *Krt5*$^{+}$ basal cells or
128 *Scgb1a1*$^{+}$ club cells, beginning segregation at E15.5 and becoming more apparent after
129 E16.5 (Figure 1C). The detection of gene signatures of NE cells, such as *Ascl1* and *Cgrp*,
130 at E13.5 (Figures 1D and S1A) showed that the differentiation of NE cells occurred the
131 earliest among the four cell populations; this finding was consistent with a previous study
132 (Linnoila, 2006).

133 **Binary cell fate decision between *Krt17*$^{+}$ basal or *Scgb3a2*$^{+}$ luminal intermediate**
134 **progenitors in primordial progenitors.**

135 We sought a novel maker for basal progenitor more committed to the basal lineage than

136 p63-expressing cells, and Krt17 was selected as a candidate (Supplementary Table 1).
137 scRNA-seq data and immunostaining revealed that Krt17 mRNA and protein appear at
138 E13.5 and E14.5, respectively (Figures 1D-F). Krt17-expressing cells become committed
139 to $Krt5^{+}$ basal cells by E18.5 (Figure 1G). We used computational trajectory analyses
140 (Figures 1H and 1I) and indicated that $Krt17^{+}$ progenitors contribute cells to all three
141 major epithelial cells, including basal cells, but $Krt17^{-}$ progenitors do not become basal
142 cells. Therefore, Krt17 expression is a novel maker for intermediate population in the
143 basal cell lineage.

144 To validate Krt17 as a novel maker for intermediate population in the basal cell lineage,
145 we conducted in vivo lineage tracing experiment with $Krt17^{CreERT2}$ $Rosa26^{mTmG/+}$ mice
146 (Doucet, et al., 2013). A total of 96.8% ± 2.9% (mean ± SD) of $Krt17^{+}$ progenitors at
147 E14.5 became mature basal cells at E18.5 (Figures 1J-L), indicating that almost all the
148 $Krt17^{+}$ cells at E14.5 have already committed toward basal cells. Thus, the expression of
149 *Krt17* is an important step for commitment to mature basal cells after the expression of
150 *p63* (Figure 2G).

151 We further identified Scgb3a2 as a marker gene for $Krt17^{-}$ progenitors by reanalyzing
152 the scRNA-seq data (Figures S2A-C). Scgb3a2 appears from E14.5 on in a pattern
153 mutually exclusive with Krt17 (Figures 2B and S2B), which suggests that equivalent

154 airway progenitors make binary cell fate decision around E14.5 to acquire either Krt17^{+}
155 or Scgb3a2^{+} (Krt17^{-}) status that do or do not differentiate into basal cells, respectively.
156 Next, we searched for a cellular signaling pathway that played a critical role in the binary
157 cell fate decision between *Krt17*$^{+}$ and *Scgb3a2*$^{+}$ progenitors and focused on Notch
158 signaling because Scgb3a2 occurs downstream of it (Guha, et al., 2012). To confirm the
159 role of Notch signaling in the cell fate decision, we genetically ablated Rbpj, a cofactor
160 of Notch signaling, in endodermal epithelium by generating *Shh*^{Cre}, *Rbpj*$^{flox/flox}$ mice
161 (RBPj cKO). In this mutant, the complete loss of Scgb3a2 is accompanied by the
162 expression of Krt17 at E16.5 in almost all epithelial cells (Figure 2C). Thus, Notch
163 signaling regulates this binary cell fate decision by inhibiting basal cell specification.

164 We further asked whether Notch activated cells during development do give rise to
165 luminal cells only, never to basal cells. Given that Notch2 is a major receptor in airway
166 progenitors(Morimoto, et al., 2012), we employed *N2IP::Cre, Rosa*$^{Ai3/+}$ mice in which
167 progeny of cells with Notch2 activation expresses a yellow fluorescent protein
168 (EYFP)(Liu, et al., 2013). As expected, EYFP-expressing cells contributed equally to
169 club and ciliated cells but never to basal cells (Figures 2D-F), confirming that Notch-
170 mediated lateral inhibition segregates primordial airway progenitors into Krt17^{+} and
171 Scgb3a2^{+} cells.

Collectively, our time series scRNA-seq analyses show that the gene signature of NE cells is first established at approximately E13.5. The remaining progenitors begin to produce two intermediate progenitors, *Krt17*$^{+}$ and *Scgb3a2*$^{+}$, around E14.5 by Notch-mediated lateral inhibition. Basal cell fate is restricted to *Krt17*$^{+}$ cells at E14.5, and a mature gene signature such as Krt5 is established at approximately E16.5 (Figure 2G).

Cell cycle slowdown induces basal cell specification concomitant with downregulation of *Id* gene expression

To elucidate the temporal regulation of epithelial progenitors' progression into slow-cycling state, we analyzed the scRNA-seq dataset with the Seurat package on the basis of enrichment of cell cycle marker expression. A substantial decrease in numbers of proliferating cells in S and G2-M phases was observed from E14.5 (Figures 3A and 3B), consistent with *in vivo* cell cycle analysis using Fucci mice (*Shh-Cre, Rosa*$^{H2B\text{-}EGFP/FucciG1}$). Numbers of cells in G0 phase (quiescent state) significantly increased between E14.5 and E16.5 (5.9% ± 1.8% vs. 22.5% ± 3.3%, mean ± SD) (Figure S2D). A BrdU incorporation assay with mouse embryos also showed a substantial decrease in the ratio of proliferative cells from E14.5 to E16.5 (54.0% ± 2.1% vs. 14.3% ± 3.6%, mean ± SD) (Figures 3C and 3D). Additionally, p63^{+} cells showed a faster decrease in BrdU incorporation than p63^{-} cells (Figure S2E). These results suggest that cell cycle slowdown preferentially occurs

190 in p63^{+} progenitors before the complete commitment into basal cell lineage and
191 subsequently induces Krt17 expression. Based on these results, we hypothesize that
192 epithelial quiescence occurs before basal cell specification.

193 We tested this hypothesis with *ex vivo* culture of E12.5 developing trachea, where
194 epithelial cells are highly proliferative and do not show any lineage commitment, with
195 and without PD0332991 (Cdk4/6 inhibitor, hereafter Cdk4/6i). Cdk4/6i inhibitor
196 treatment induces cell cycle arrest at the G1 phase and the differentiation into *Krt17*$^{+}$ cells
197 in a dose-dependent manner (Figures 3E and 3F). Furthermore, Scgb3a2 cells were
198 significantly increased following Cdk4/6i treatment (Figures 3G and 3H). Hence, cell
199 cycle arrest in epithelial progenitors is sufficient to induce basal cell specification and
200 promote differentiation of Krt17^{+} basal progenitors.

201 To identify transcription factors (TFs) related to the epithelial cell cycle slowdown, we
202 repeated cluster analysis using all 1385 genes, which are classified as TFs in Fantom5
203 SSTAR database (Figures 3I and 3J) (Abugessaisa, et al., 2016). The cells showed similar
204 TF profiles at E12.5 and E13.5 but dynamically changed their TF profiles between E14.5
205 and E16.5, establishing distinct lineage-specific profiles. We focused on genes with
206 expression levels that substantially changed at E14.5 and noted inhibitors of DNA-
207 binding/differentiation genes (*Id1*, *Id2*, and *Id3*) (Figure S2F). Generally, Id proteins

208 promote proliferation by antagonizing negative cell cycle regulators, such as Rb, and
209 simultaneously inhibit differentiation by binding with various bHLH-type TFs(Roschger
210 and Cabrele, 2017; Lasorella, et al., 2014). *Id4* was not detected in our dataset, yet the
211 expression of *Id1*, *Id2*, and *Id3* was abundant in progenitors until E14.5 and then
212 decreased along with the slowing of the cell cycle (Figure 3K). This temporal reduction
213 in expression of *Id* genes was confirmed with proximity ligation *in situ* hybridization
214 (PLISH)(Nagendran, et al., 2018) and dot quantification (Figures 3L and 3M). $Ki67^{+}$
215 proliferative cells preferentially express *Id2* gene (Figure 3N) and *Id* genes expression
216 was lower in $Krt17^{+}$ cells than $Krt17^{-}$ cells at E14.5 (Figure S2G). These observations are
217 consistent with the hypothesis that the reduction in *Id* expression is involved in cell cycle
218 slowdown in tracheal epithelium, which triggers the basal cell specification.

219 **_Id2_ downregulation promotes basal cell specification of epithelial progenitors**
220 **through cell cycle modulation**

221 Next, to confirm the roles of *Id* genes in modulating epithelial cell cycle and basal cell
222 specification, we used *Id2* loss- and gain-of-function transgenic mice. $Id2^{CreERT2/CreERT2}$
223 mice were used as *Id2* knockout mice (*Id2* KO mice)(Rawlins, et al., 2009) (Figures S3C
224 and S3D). BrdU incorporation assays with *Id2* KO mice showed a significant decrease in
225 proliferating cells at E14.5 and E15.5 (Figures 4A and S3A). Additionally, both $Krt17^{+}$

and Scgb3a2^{+} progenitors were detected earlier in *Id2* KO mice than in control mice (Figure 4B). Thus, the loss of *Id2* appears to accelerate airway progenitor specification by lowering the proliferation rate. *Shh^{Cre}, Rosa$^{3xHA\text{-}Id2\text{-}IRES\text{-}H2B\text{-}EGFP}$* mice (*Id2* OE) that overexpress *Id2* in endodermal epithelial cells (Figures S3E and S3F) significantly increased *Ki67^{+}* proliferative cells at E14.5 and E16.5 (Figures 4C and S3B) and decreased both *Krt17^{+}* and *Scgb3a2^{+}* progenitors at E14.5 (Figures 4C and 4D). Based on these observations, we conclude that the temporal regulation of Id2 dosage determines the timing of the epithelial cell cycle and basal cell specification.

Mesenchymal-to-epithelial Tgfß signaling initiates cell cycle slowdown in epithelial cells by suppressing the *Id2* gene

Since *Id* genes are known to be downstream factors of Tgfβ signaling in hematopoietic cells (Roschger and Cabrele, 2017; Lasorella, et al., 2014), we evaluated the effects of Tgfβ signaling on *Id* genes using *Shh^{Cre}*, *Tgfbr2$^{flox//flox}$* mice in which the *Tgfβ receptor 2* gene is ablated in the endodermal epithelium (*Tgfbr2* cKO). The *Id2* gene expression was significantly upregulated in the *Tgfbr2* cKO mice at E14.5 (Figure 4E), suggesting that Tgfβ inhibits *Id2* expression. Consistent with the enhanced *Id2* phenotype, epithelial cells in *Tgfbr2* cKO mice showed more *Ki67^{+}* proliferative cells and a more delayed appearance of *Krt17^{+}* progenitors than those in the control mice (Figure 4F). At E18.5,

Tgfbr2 cKO mice showed a significant decrease in mature *Krt5*$^{+}$ basal cells (Figure 4G), indicating that *Tgfbr2* activation is involved in basal cell specification by inhibiting *Id2* expression. These findings are consistent with the previous report that Smad activation through Tgfβ signaling is necessary for the specification of human *p63*$^{+}$ basal cell population from *Id2*$^{+}$ primordial progenitors (Miller, et al., 2020). *Ex vivo* trachea culture with Tgfß ligands (Tgfβ-1/2/3) confirms that Tgfβ ligand inhibits *Id2* expression, forces epithelial cells into slow cycling, and induces more *Krt17*$^{+}$ cells than Tgfβ inhibitor (SB431542) (Figures 4H-J). Hence, we propose that Tgfβ signaling acts as the initial cue for the epithelial cell cycle slowdown and the specification of the *Krt17*$^{+}$ basal progenitors by decreasing *Id2* gene expression.

Next, we investigated Tgfβ ligand-secreting cells with PLISH and found that mesenchymal cells express *Tgfβ-3* throughout development (Figure S4A). The number of Tgfβ-3-secreting cells decrease over time, but subepithelial mesenchymal cells are positive for *Tgfβ-3* even at E18.5. Thus, it is highly likely that airway mesenchyme is the major source of the Tgfβ ligand.

_Id2_ expression in mature basal stem cells ensures their proliferative potential at perinatal and adult stages

While we showed that *Id2* attenuation is the key step for the specification of basal cell progenitors in development, the predominant expression of *Id* genes in mature basal cells has been reported in adulthood (Montoro et al., 2019). We compared *Id2* expression between basal and luminal cells isolated from Krt17-EGFP transgenic mice (Bianchi, et al., 2005) at E18.5 using qRT-PCR and confirmed twofold higher expression of *Id2* in basal cells in compare to luminal cells (Figure 5A). Therefore, next, we asked whether the *Id2* gene's function in regulating proliferation during development was conserved at perinatal and adult stages. We employed a tracheosphere culture assay and estimated the colony-forming efficiency (CFE) in *Id2* KO, control, and *Id2* OE mice at E18.5 (Figure 5B). The epithelial cells from the *Id2* OE mice showed a significantly higher CFE than those in other groups, suggesting that the Id2 dosage was related to the proliferative capacity of epithelial cells at the perinatal stage. The predominant expression of *Id2* in basal cells was also detected in 2-month-old adult mice (Figure 5A). Similar to E18.5, basal cells from *Id2* OE mice showed a significantly higher CFE than those in the control group (Figure 5C). These results confirm that the Id2 dosage ensures the self-renewal capacity of basal cells at perinatal and adult stages.

The slow-cycling basal cells re-enter the cell cycle with recurrent *Id2* activation following injury

279 Next, we asked whether *Id2* was involved in airway tissue regeneration at the adult stage.
280 SO_2-inhalation mediated airway injury can be used as a model to study basal cell-driven
281 airway epithelial regeneration (Pardo-Saganta, et al., 2015; Rawlins, et al., 2007;
282 Borthwick, et al., 2001). Therefore, we used this model to assess the airway epithelial
283 regeneration process. The number of Ki67-expressing cells started increasing at 18 h
284 post-injury (hpi), and peaked at approximately 24 hpi (Figure 6A), suggesting that the
285 transition of basal cells from slow-cycling to active proliferation occurs around 18 hpi.
286 An increase in *Id2* expression was detected at 12 hpi before the increase in Ki67-
287 expressing cells (Figure 6B). These observations prompted us to hypothesize that
288 recurrent Id2 activation stimulated basal cells to re-enter the active cell cycle. We exposed
289 wild-type and *Id2* OE adult mice to SO_2 gas and examined their respective number of
290 Ki67-expressing cells to test this hypothesis. Airways from the *Id2* OE mice showed a
291 more rapid response to injury than airways from wild-type mice at 12 hpi (Figure 6C),
292 indicating the artificially increased *Id2* expression enhances basal cell proliferation.
293 Additionally, *Id2* OE prolonged the proliferation of $Krt5^+$ basal cells more than 72 hpi
294 and prohibited basal cell differentiation into $Krt5^-$ luminal cells, showing the phenotype
295 similar to basal cell hyperplasia, a precancer-like state (Figure 6C). These results imply
296 that high *Id2* expression in airway epithelial cells promoted the transition of basal cells

297 from the slow-cycling to the active proliferation state; in contrast, sustained *Id2*
298 expression inhibits a return from the active proliferation state to the slow-cycling state.
299 Thus, *Id2* is a key factor in regulating basal cells' transition from slow cycling to
300 proliferation in response to epithelial damage and inhibiting their differentiation into
301 luminal cells.

302 **The inhibitory effect of Tgfβ signaling on Id2 expression is conserved until adult**
303 **stages**

304 Lastly, we attempted to determine that the inhibitory effect of Tgfβ signaling on Id2
305 expression in lung development is conserved at perinatal and adult stages. First, we
306 checked the expression pattern of pSmad2/3 at E18.5, which is downstream of Tgfβ
307 signaling. Consistent with predominant *Id2* expression in mature basal cell population,
308 pSmad2/3 expression is significantly lower in mature basal cells than luminal cells
309 (Figure 7A). In addition, Tgfβ superfamily signaling inhibitors, such as *Tgif1*, *Nbl1*,
310 *Sostdc1*, and *Fst* are highly and exclusively expressed in basal cell population (Figures
311 S5A-F). These observations suggest that basal cells may express Tgfβ inhibitors to inhibit
312 Tgfβ signaling and maintain *Id2* expression. Supporting this idea, dual Smad inhibition
313 via Tgfβ/Bmp inhibitors is beneficial for the maintenance of mature basal cells (Mou, et
314 al., 2016; Tadokoro, et al., 2016). The inhibitory effect of Tgfβ signaling on *Id2*

315 expression was directly confirmed by the basal cell culture with Tgfβ ligands (Tgfß-1/2/3)
316 or inhibitor (SB431542) (Figure 7B). Tgfβ ligands treatment significantly decreased *Id2*
317 expression in basal cell culture.

318 We further assess the function of Tgfβ signaling in *in vivo* tissue regeneration process.
319 *Tgfβ–3* and pSmad2/3 expression after SO_2 injury was monitored with PLISH and
320 immunostaining, respectively. *Tgfβ–3* expression was significantly decreased after SO_2
321 injury (Figures 7C and 7D), consistent with the decreased pSmad2/3 intensity in both
322 epithelial and mesenchymal cells. Furthermore, *Tgfbr2* cKO mice at 72 hpi also showed
323 increased *Id2* expression (Figure 7F) as well as basal cell hyperplasia, the phenocopy of
324 *Id2* OE mice (Figure 7E). Thus, the Tgfβ-Id2 axis is likely a critical regulator of the
325 transition between the active proliferation and the slow-cycling state, which is conserved
326 during development and adult tissue regeneration, in airway stem cells.

327

328 **Discussion**

329 In the present study, we investigated the conserved mechanism regulating the
330 proliferation mode transitions of airway basal stem cells in development and
331 regeneration; we also found that Tgfβ-Id2 axis is a commonly shared regulator in both

these processes. During basal cell specification in airway development, *Id2* attenuation triggered by mesenchymal-to-epithelial Tgfβ signaling slows down epithelial progenitors' cell cycle and induces the *Krt17*$^{+}$ basal progenitors. *Id2* expression ensures mature basal cells' capacity for self-renewal in a dose-dependent manner. In the adult tissue regeneration model, the recurrent activation of *Id2* via Tgfβ reduction initiates tissue regeneration by forcing the slow-cycling basal cell to re-enter the active cell cycle. While proliferating basal cells get back to the slow-cycling state by 120 hpi in normal tissue regeneration, enhanced *Id2* expression or impaired Tgfβ receptor results in basal cell hyperplasia that resembles a precancerous condition (Figure 7G).

Basal cells' tightly regulated proliferative potential is critical for tissue regeneration, homeostasis, and the avoidance of pathological conditions. Airway basal cells remain quiescent under homeostasis; in response to injury, they re-enter the cell cycle to replenish the lost cells by producing transit-amplifying cells. However, excessive proliferation is related to squamous cell carcinoma (Lapouge, et al., 2011). Recently, there has been increasing evidence of tumor cells, including lung cancer cells, hijacking the embryonic pathways, which control stem and progenitor cell behavior during development (Laughney, et al., 2020; Tata, et al., 2018; Murry and Keller, 2008). Following this concept, we demonstrated that mature basal stem cells reutilized the Tgfβ-Id2 axis in

350 tissue regeneration for the tightly regulated transitions between slow-cycling and
351 proliferation. During development, the Tgfβ-Id2 axis also plays critical roles in regulating
352 the cell cycle state for the specification of slow-cycling basal progenitors.

353 The acquisition of cellular quiescence in stem cell development has been reported in
354 mammalian neurogenesis (Furutachi, et al., 2015). A subset of embryonic neuroepithelial
355 cells slows cell cycling between E13.5 and E15.5, isolating a population of primordial
356 neural stem cells. The expression of the cyclin-dependent kinase inhibitor, p57,
357 demarcates primordial neural stem cells from non-stem cells and defines reversible
358 quiescence status and specification numbers of adult neural stem cells. The embryonic
359 origin of adult stem cells could acquire quiescence by reducing the number of divisions
360 at an early stage of development to prevent the exhaustion of the stem cell pool. (Cheung
361 and Rando, 2013).

362 Id2 was first reported as a marker of multipotent cells at the distal tip region of
363 developing lungs(Rawlins, et al., 2009). This region includes highly self-renewing
364 progenitors. However, Id2 function in airway stem cell is still to be determined. We show
365 that *Id2* is highly expressed in primordial progenitors in developing airways until E14.5
366 (Figures 3J-M). Generally, *Id* genes display two direct effects on proliferation and
367 differentiation via independently interacting with negative cell cycle regulators, such as

368 Rb, and differentiation-related TFs, such as bHLH-type TFs(Roschger and Cabrele, 2017;
369 Lasorella, et al., 2014). *Id* gene dosage during airway development could determine the
370 proliferation state because *Id2* loss-of-function transgenic mice show advanced cell cycle
371 attenuation and basal cell specification. In contrast, these processes were delayed in *Id2*
372 gain-of-function transgenic mice (Figures 4A and 4C). We cannot exclude the possibility
373 that Id2 directly inhibits key TFs for epithelial differentiation, although we did not detect
374 any bHLH-type TFs as promising candidates in our scRNA-seq data. In future studies, a
375 comprehensive screening assay is required to confirm the existence of specific TFs
376 responsible for epithelial differentiation.

377 TGF superfamily signaling is reported to induce stem cell quiescence in various
378 organs(Genander, et al., 2014; Kandasamy, et al., 2014; Nishimura, et al., 2010; Yamazaki,
379 et al., 2009). In the present study, we showed that Tgfβ signaling initiates the transition
380 in airway epithelial cells from the active proliferation to the slow-cycling state by
381 suppressing *Id2* expression; this transition is most likely conserved during both
382 development and regeneration. Generally, Tgfβ activates or suppresses *Id* genes context-
383 dependently(Roschger and Cabrele, 2017; Lasorella, et al., 2014). Tgfβ inhibits *Id* genes
384 in basal keratinocytes that are similar to airway basal cells(Rotzer, et al., 2006). This
385 inhibitory effect of Tgfβ is also consistent with dual inhibition of Tgfβ/BMP signaling

386 that promotes self-renewal of the basal cell population(Mou, et al., 2016; Tadokoro, et al.,
387 2016). However, the precise molecular mechanism how Tgfβ signaling inhibits *Id2*
388 expression is still to be elucidated.

389 The present study shows that mature basal cells maintain moderate Id2 expression to
390 ensure proliferative potential at perinatal and adult stages (Figure 5A). Our organoid
391 culture experiments confirmed the positive function of *Id2* in epithelial proliferation
392 (Figures 5B and 5C), indicating that *Id2* has a consistent function in basal cell lineage to
393 promote proliferation in a dose-dependent manner (Figure 7G). This critical role of Id
394 genes is conserved in neural and hematopoietic stem cells(Jung, et al., 2010; Jankovic, et
395 al., 2007). Additionally, Id2 dosage directly affects the normal repair processes in
396 response to SO_2 injury (Figure 6C). After SO_2 injury, the artificial enhancement of the
397 *Id2* gene accelerates tissue regeneration, but aberrant *Id2* gene expression results in
398 premalignant basal cell hyperplasia seen in *Id2* OE mice. Thus, the tight regulation of Id2
399 is needed for normal tissue regeneration prohibiting pathological conditions due to
400 sustained proliferation. Consistent with this conclusion, aberrant Id genes expression is
401 observed in cancer cells in various organs, especially in cancer stem cells including the
402 lungs, contributing to the tumorigenesis and metastasis (Roschger and Cabrele, 2017;
403 Lasorella, et al., 2014; Pillai, et al., 2011).

In addition, the fact that Tgfbr2 cKO mice phenocopied Id2 OE mice after SO_2 injury demonstrated that Tgfβ signaling governs tissue regeneration via controlling proliferative states of basal stem cells through tight regulation of Id2 expression (Figures 7E and 7F). Thus, fine tuning of Tgfβ-Id2 axis is a key for proper recovery from severe tissue damage caused by influenza virus or SARS-CoV-2 and represents a possible therapeutic target in squamous lung carcinoma.

Acknowledgments

We thank David M. Owens for the Krt17-CreER mice, Tasuku Honjo for the Rbpj flox mice, Raphael Kopan for the N2IP::Cre mice and the Animal Resource Development Unit. We also thank Kuraku Shigehiro, Kadota Mitsuru, Nishimura Osamu, Quan Wu, and Miura Hisashi for assistance with the scRNA-seq data analysis. We thank Raphael Kopan and Hiroshi Hamada for reviewing the manuscript.

These studies are supported by funding from Grants-in-Aid for Scientific Research (B) (20H03693) (M.M.), Young Scientists (19K17691) (K.H.) of the Ministry of Education, and Culture, Sports, Science and Technology, Japan; from RIKEN BDR-Otsuka Pharmaceutical Collaboration Center (RBOC) and from the Special Postdoctoral

Researcher (SPDR) Program of RIKEN (H.K.).

Author contributions

K.H. and M.M. designed the project and performed experiments with the aid of Y.A. and M.C. K.H. analyzed the single-cell transcriptomics data from embryonic and adult tracheal epithelium. Y.A. assisted with the mouse experiments. M.C. supported the generation of LSL-Id2-IRES-H2B-EGFP. A.T. and K.H. generated the Rosa26$^{LSL\text{-}Id2\text{-}IRES\text{-}H2B\text{-}EGFP}$ animals. K.H. and M.M. wrote the manuscript with the contribution of all authors.

Abugessaisa, I., Shimoji, H., Sahin, S., Kondo, A., Harshbarger, J., Lizio, M., Hayashizaki, Y., Carninci, P., consortium, F., Forrest, A., et al. (2016). FANTOM5 transcriptome catalog of cellular states based on Semantic MediaWiki. Database (Oxford) 2016.

Arner, E., Daub, C.O., Vitting-Seerup, K., Andersson, R., Lilje, B., Drablos, F., Lennartsson, A., Ronnerblad, M., Hrydziuszko, O., Vitezic, M., et al. (2015). Transcribed enhancers lead waves of coordinated transcription in transitioning mammalian cells. Science 347, 1010-4.

Barker, N., Ridgway, R.A., van Es, J.H., van de Wetering, M., Begthel, H., van den Born, M., Danenberg, E., Clarke, A.R., Sansom, O.J., and Clevers, H. (2009). Crypt stem cells as the cells-of-origin of intestinal cancer. Nature 457, 608-11.

Bianchi, N., Depianto, D., McGowan, K., Gu, C., and Coulombe, P.A. (2005). Exploiting the keratin 17 gene promoter to visualize live cells in epithelial appendages of mice. Mol Cell Biol 25, 7249-59.

Blenkinsopp, W.K. (1967). Proliferation of respiratory tract epithelium in the rat. Exp Cell Res 46, 144-54.

Borthwick, D.W., Shahbazian, M., Krantz, Q.T., Dorin, J.R., and Randell, S.H. (2001). Evidence for stem-cell niches in the tracheal epithelium. Am J Respir Cell Mol Biol 24, 662-70.

Cheung, T.H., and Rando, T.A. (2013). Molecular regulation of stem cell quiescence. Nat Rev Mol Cell Biol 14, 329-40.

446 **Consortium, F., the, R.P., Clst, Forrest, A.R., Kawaji, H., Rehli, M., Baillie, J.K., de Hoon, M.J., Haberle, V.,**
447 **Lassmann, T., et al. (2014). A promoter-level mammalian expression atlas. Nature 507, 462-70.**
448 **Desai, T.J., Brownfield, D.G., and Krasnow, M.A. (2014). Alveolar progenitor and stem cells in lung**
449 **development, renewal and cancer. Nature 507, 190-4.**
450 **Doucet, Y.S., Woo, S.H., Ruiz, M.E., and Owens, D.M. (2013). The touch dome defines an epidermal niche**
451 **specialized for mechanosensory signaling. Cell Rep 3, 1759-65.**
452 **Feitelson, M.A., Arzumanyan, A., Kulathinal, R.J., Blain, S.W., Holcombe, R.F., Mahajna, J., Marino, M.,**
453 **Martinez-Chantar, M.L., Nawroth, R., Sanchez-Garcia, I., et al. (2015). Sustained proliferation in cancer:**
454 **Mechanisms and novel therapeutic targets. Semin Cancer Biol 35 Suppl, S25-S54.**
455 **Furutachi, S., Miya, H., Watanabe, T., Kawai, H., Yamasaki, N., Harada, Y., Imayoshi, I., Nelson, M., Nakayama,**
456 **K.I., Hirabayashi, Y., et al. (2015). Slowly dividing neural progenitors are an embryonic origin of adult neural**
457 **stem cells. Nat Neurosci 18, 657-65.**
458 **Gancz, D., Lengil, T., and Gilboa, L. (2011). Coordinated regulation of niche and stem cell precursors by**
459 **hormonal signaling. PLoS Biol 9, e1001202.**
460 **Genander, M., Cook, P.J., Ramskold, D., Keyes, B.E., Mertz, A.F., Sandberg, R., and Fuchs, E. (2014). BMP**
461 **signaling and its pSMAD1/5 target genes differentially regulate hair follicle stem cell lineages. Cell Stem Cell**
462 **15, 619-33.**
463 **Guha, A., Vasconcelos, M., Cai, Y., Yoneda, M., Hinds, A., Qian, J., Li, G., Dickel, L., Johnson, J.E., Kimura, S.,**
464 **et al. (2012). Neuroepithelial body microenvironment is a niche for a distinct subset of Clara-like precursors**
465 **in the developing airways. Proc Natl Acad Sci U S A 109, 12592-7.**
466 **Herriges, M., and Morrisey, E.E. (2014). Lung development: orchestrating the generation and regeneration**
467 **of a complex organ. Development 141, 502-13.**
468 **Hogan, B.L., Barkauskas, C.E., Chapman, H.A., Epstein, J.A., Jain, R., Hsia, C.C., Niklason, L., Calle, E., Le, A.,**
469 **Randell, S.H., et al. (2014). Repair and regeneration of the respiratory system: complexity, plasticity, and**
470 **mechanisms of lung stem cell function. Cell Stem Cell 15, 123-38.**
471 **Hong, K.U., Reynolds, S.D., Watkins, S., Fuchs, E., and Stripp, B.R. (2004). Basal cells are a multipotent**
472 **progenitor capable of renewing the bronchial epithelium. Am J Pathol 164, 577-88.**
473 **Jankovic, V., Ciarrocchi, A., Boccuni, P., DeBlasio, T., Benezra, R., and Nimer, S.D. (2007). Id1 restrains myeloid**
474 **commitment, maintaining the self-renewal capacity of hematopoietic stem cells. Proc Natl Acad Sci U S A 104,**
475 **1260-5.**
476 **Jung, S., Park, R.H., Kim, S., Jeon, Y.J., Ham, D.S., Jung, M.Y., Kim, S.S., Lee, Y.D., Park, C.H., and Suh-Kim, H.**
477 **(2010). Id proteins facilitate self-renewal and proliferation of neural stem cells. Stem Cells Dev 19, 831-41.**
478 **Kandasamy, M., Lehner, B., Kraus, S., Sander, P.R., Marschallinger, J., Rivera, F.J., Trumbach, D., Ueberham, U.,**
479 **Reitsamer, H.A., Strauss, O., et al. (2014). TGF-beta signalling in the adult neurogenic niche promotes stem**
480 **cell quiescence as well as generation of new neurons. J Cell Mol Med 18, 1444-59.**
481 **Kiyokawa, H., and Morimoto, M. (2020). Notch signaling in the mammalian respiratory system, specifically**

482 **the trachea and lungs, in development, homeostasis, regeneration, and disease. Dev Growth Differ 62, 67-**
483 **79.**
484 **Kotton, D.N., and Morrisey, E.E. (2014). Lung regeneration: mechanisms, applications and emerging stem**
485 **cell populations. Nat Med 20, 822-32.**
486 **Lapouge, G., Youssef, K.K., Vokaer, B., Achouri, Y., Michaux, C., Sotiropoulou, P.A., and Blanpain, C. (2011).**
487 **Identifying the cellular origin of squamous skin tumors. Proc Natl Acad Sci U S A 108, 7431-6.**
488 **Lasorella, A., Benezra, R., and Iavarone, A. (2014). The ID proteins: master regulators of cancer stem cells**
489 **and tumour aggressiveness. Nat Rev Cancer 14, 77-91.**
490 **Laughney, A.M., Hu, J., Campbell, N.R., Bakhoum, S.F., Setty, M., Lavallee, V.P., Xie, Y., Masilionis, I., Carr, A.J.,**
491 **Kottapalli, S., et al. (2020). Regenerative lineages and immune-mediated pruning in lung cancer metastasis.**
492 **Nat Med 26, 259-269.**
493 **Leach, J.P., and Morrisey, E.E. (2018). Repairing the lungs one breath at a time: How dedicated or facultative**
494 **are you? Genes Dev 32, 1461-1471.**
495 **Linnoila, R.I. (2006). Functional facets of the pulmonary neuroendocrine system. Lab Invest 86, 425-44.**
496 **Liu, Z., Chen, S., Boyle, S., Zhu, Y., Zhang, A., Piwnica-Worms, D.R., Ilagan, M.X., and Kopan, R. (2013). The**
497 **extracellular domain of Notch2 increases its cell-surface abundance and ligand responsiveness during kidney**
498 **development. Dev Cell 25, 585-98.**
499 **Mikkola, H.K., and Orkin, S.H. (2006). The journey of developing hematopoietic stem cells. Development 133,**
500 **3733-44.**
501 **Miller, A.J., Yu, Q., Czerwinski, M., Tsai, Y.H., Conway, R.F., Wu, A., Holloway, E.M., Walker, T., Glass, I.A.,**
502 **Treutlein, B., et al. (2020). In Vitro and In Vivo Development of the Human Airway at Single-Cell Resolution.**
503 **Dev Cell.**
504 **Morimoto, M., Liu, Z., Cheng, H.T., Winters, N., Bader, D., and Kopan, R. (2010). Canonical Notch signaling in**
505 **the developing lung is required for determination of arterial smooth muscle cells and selection of Clara versus**
506 **ciliated cell fate. J Cell Sci 123, 213-24.**
507 **Morimoto, M., Nishinakamura, R., Saga, Y., and Kopan, R. (2012). Different assemblies of Notch receptors**
508 **coordinate the distribution of the major bronchial Clara, ciliated and neuroendocrine cells. Development 139,**
509 **4365-73.**
510 **Morrisey, E.E., and Hogan, B.L. (2010). Preparing for the first breath: genetic and cellular mechanisms in**
511 **lung development. Dev Cell 18, 8-23.**
512 **Mou, H., Vinarsky, V., Tata, P.R., Brazauskas, K., Choi, S.H., Crooke, A.K., Zhang, B., Solomon, G.M., Turner,**
513 **B., Bihler, H., et al. (2016). Dual SMAD Signaling Inhibition Enables Long-Term Expansion of Diverse**
514 **Epithelial Basal Cells. Cell Stem Cell 19, 217-231.**
515 **Murry, C.E., and Keller, G. (2008). Differentiation of embryonic stem cells to clinically relevant populations:**
516 **lessons from embryonic development. Cell 132, 661-80.**
517 **Nagendran, M., Riordan, D.P., Harbury, P.B., and Desai, T.J. (2018). Automated cell-type classification in intact**

518 **tissues by single-cell molecular profiling. Elife 7.**

519 **Nishimura, E.K., Suzuki, M., Igras, V., Du, J., Lonning, S., Miyachi, Y., Roes, J., Beermann, F., and Fisher, D.E.**
520 **(2010). Key roles for transforming growth factor beta in melanocyte stem cell maintenance. Cell Stem Cell 6,**
521 **130-40.**

522 **Nowak, J.A., Polak, L., Pasolli, H.A., and Fuchs, E. (2008). Hair follicle stem cells are specified and function**
523 **in early skin morphogenesis. Cell Stem Cell 3, 33-43.**

524 **Pardo-Saganta, A., Law, B.M., Tata, P.R., Villoria, J., Saez, B., Mou, H., Zhao, R., and Rajagopal, J. (2015).**
525 **Injury induces direct lineage segregation of functionally distinct airway basal stem/progenitor cell**
526 **subpopulations. Cell Stem Cell 16, 184-97.**

527 **Pillai, S., Rizwani, W., Li, X., Rawal, B., Nair, S., Schell, M.J., Bepler, G., Haura, E., Coppola, D., and Chellappan,**
528 **S. (2011). ID1 facilitates the growth and metastasis of non-small cell lung cancer in response to nicotinic**
529 **acetylcholine receptor and epidermal growth factor receptor signaling. Mol Cell Biol 31, 3052-67.**

530 **Rawlins, E.L., Clark, C.P., Xue, Y., and Hogan, B.L. (2009). The Id2+ distal tip lung epithelium contains**
531 **individual multipotent embryonic progenitor cells. Development 136, 3741-5.**

532 **Rawlins, E.L., Ostrowski, L.E., Randell, S.H., and Hogan, B.L. (2007). Lung development and repair:**
533 **contribution of the ciliated lineage. Proc Natl Acad Sci U S A 104, 410-7.**

534 **Rock, J.R., Gao, X., Xue, Y., Randell, S.H., Kong, Y.Y., and Hogan, B.L. (2011). Notch-dependent differentiation**
535 **of adult airway basal stem cells. Cell Stem Cell 8, 639-48.**

536 **Rock, J.R., Onaitis, M.W., Rawlins, E.L., Lu, Y., Clark, C.P., Xue, Y., Randell, S.H., and Hogan, B.L. (2009). Basal**
537 **cells as stem cells of the mouse trachea and human airway epithelium. Proc Natl Acad Sci U S A 106, 12771-**
538 **5.**

539 **Roschger, C., and Cabrele, C. (2017). The Id-protein family in developmental and cancer-associated pathways.**
540 **Cell Commun Signal 15, 7.**

541 **Rotzer, D., Krampert, M., Sulyok, S., Braun, S., Stark, H.J., Boukamp, P., and Werner, S. (2006). Id proteins:**
542 **novel targets of activin action, which regulate epidermal homeostasis. Oncogene 25, 2070-81.**

543 **Shyer, A.E., Huycke, T.R., Lee, C., Mahadevan, L., and Tabin, C.J. (2015). Bending gradients: how the intestinal**
544 **stem cell gets its home. Cell 161, 569-580.**

545 **Tadokoro, T., Gao, X., Hong, C.C., Hotten, D., and Hogan, B.L. (2016). BMP signaling and cellular dynamics**
546 **during regeneration of airway epithelium from basal progenitors. Development 143, 764-73.**

547 **Tata, P.R., Chow, R.D., Saladi, S.V., Tata, A., Konkimalla, A., Bara, A., Montoro, D., Hariri, L.P., Shih, A.R., Mino-**
548 **Kenudson, M., et al. (2018). Developmental History Provides a Roadmap for the Emergence of Tumor**
549 **Plasticity. Dev Cell 44, 679-693 e5.**

550 **Yamazaki, S., Iwama, A., Takayanagi, S., Eto, K., Ema, H., and Nakauchi, H. (2009). TGF-beta as a candidate**
551 **bone marrow niche signal to induce hematopoietic stem cell hibernation. Blood 113, 1250-6.**

552 **Yang, Y., Riccio, P., Schotsaert, M., Mori, M., Lu, J., Lee, D.K., Garcia-Sastre, A., Xu, J., and Cardoso, W.V.**
553 **(2018). Spatial-Temporal Lineage Restrictions of Embryonic p63(+) Progenitors Establish Distinct Stem Cell**

554 **Pools in Adult Airways. Dev Cell 44, 752-761 e4.**

555 **Yanger, K., and Stanger, B.Z. (2011). Facultative stem cells in liver and pancreas: fact and fancy. Dev Dyn 240,**

556 **521-9.**

557

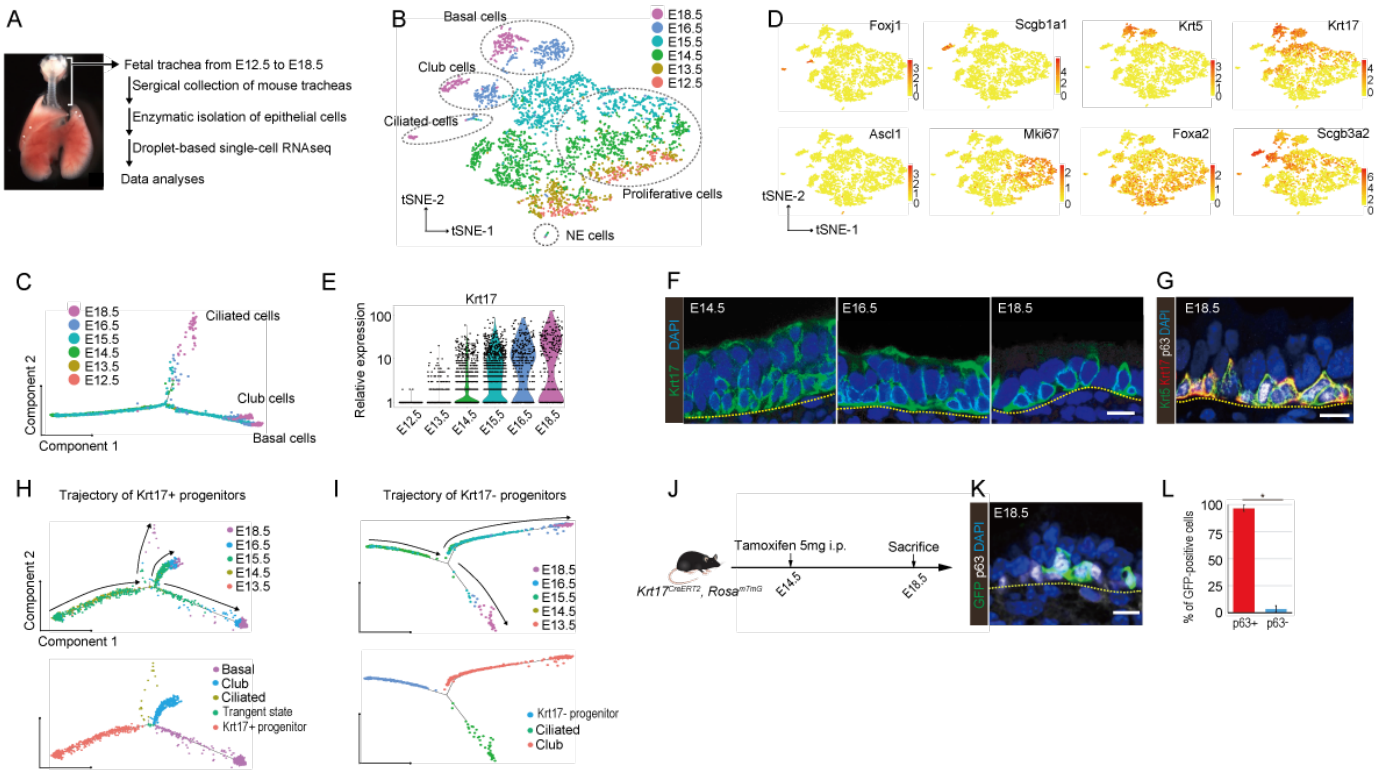

Figure 1. Time-series scRNA-seq analyses delineate a developmental roadmap of airway epithelial cells, including basal cells.

(A) Schematic representation of the time-series scRNA-seq analyses of developing tracheal epithelial cells. (B) The t-SNE plot of single cells displayed thirteen distinct clusters, including four distinct mature cell types. (C) Pseudotime analysis with the Monocle package illustrated the developmental trajectories towards three mature cell lineages. (D) Canonical marker expression in the t-SNE map. (E) The temporal expression of *Krt17* in the scRNA-seq data. (F-G) Immunostaining for Krt17 in the developing trachea confirmed the limited expression pattern in basal cells. *In silico* trajectory analyses of the *Krt17*-expressing (H) and nonexpressing progenitors (I) using Monocle. (J) Lineage tracing experiment for the Krt17^{+} progenitors at E14.5 using the *Krt17*^{CreERT2} *Rosa26*$^{mTmG/+}$ mice. (K) Immunostaining for GFP and p63 revealed that most Krt17^{+} progenitors at E14.5 contributed to p63^{+} cells at E18.5 (L) (mean±SD, n=4). * p< 0.05; Student's t test. Scale bars, 5 μm.

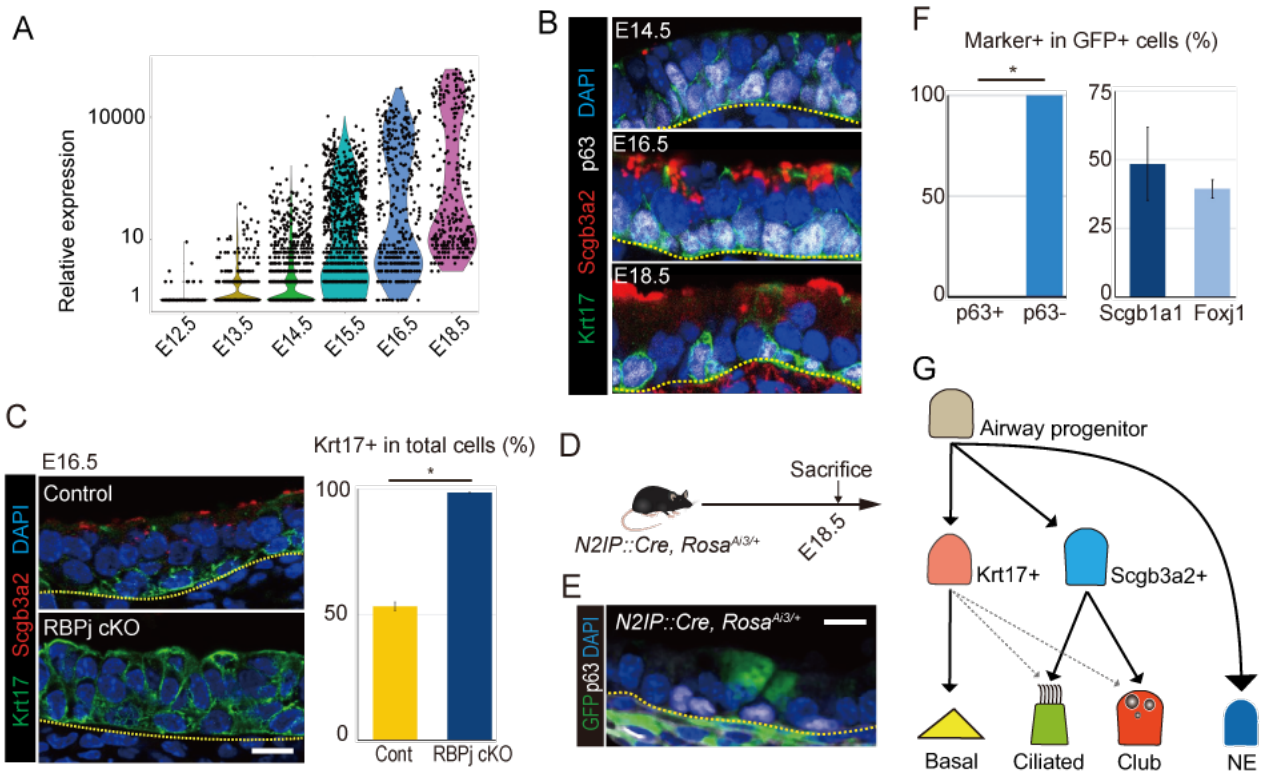

Figure 2. Binary cell fate decision between *Krt17*$^{+}$ basal or *Scgb3a2*$^{+}$ luminal intermediate progenitors in primordial progenitors.

(A) The temporal expression of *Scgb3a2* over time in the scRNA-seq dataset. (B) Actual expression patterns of Scgb3a2 and Krt17 detected by immunostaining. (C) Phenotypic analyses of the RBPj KO mice tracheas at E16.5 by immunostaining for Krt17 and Scgb3a2 revealed the expansion of Krt17^{+} progenitors at the expense of Scgb3a2^{+} progenitors. (D) The lineage tracing experiment for the progenitors that experienced Notch2 activation during development was performed with *N2IP::Cre, Rosa*$^{Ai3/+}$ mice. (E,F) Quantitative immunostaining assessment with anti-GFP antibody demonstrated their exclusive contribution to p63^{-} luminal cells at E18.5. (G) Schematic summary of the roadmap for developing airway epithelial cells showing two types of progenitors, Krt17^{+} and Scgb3a2^{+} (Krt17^{-}) progenitors.

* p< 0.05; Student's t test. Mean±SD, n=4–6 (C, F). Scale bars: 5 μm.

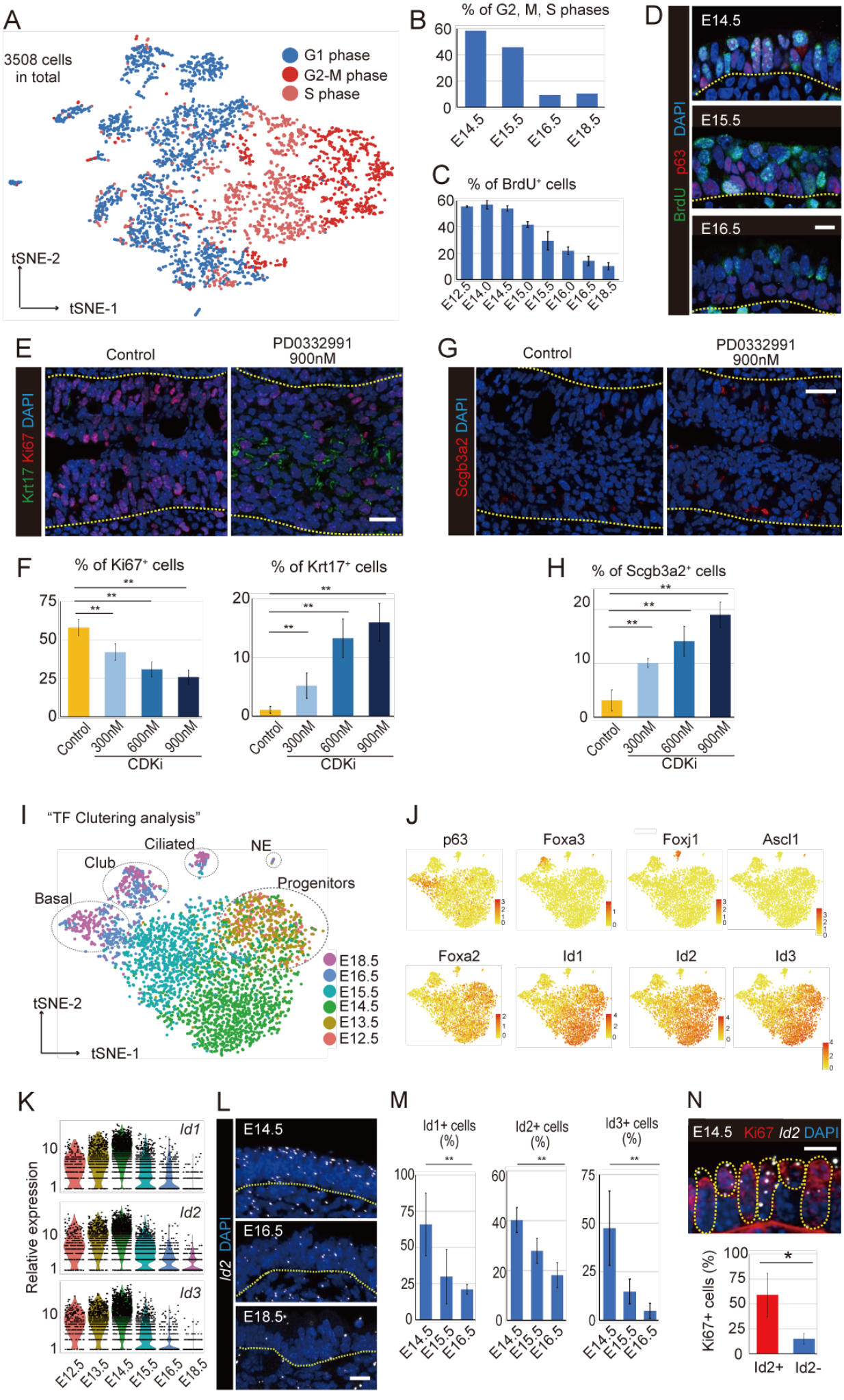

Figure 3. Cell cycle slowdown induces basal cell specification concomitant with downregulation of *Id* gene expression. (A) Cell cycle analysis with the scRNA-seq data using the Seurat package. (B) The ratio of cells expressing markers of S, G2, and M phases revealed a substantial decrease in proliferating cells from E14.5. (C-D) BrdU incorporation assay with immunostaining confirmed the cell cycle deceleration from E14.5. (E-G) Immunostaining for Krt17, Scgb3a2, and Ki67 in *ex vivo* cultured fetal tracheal epithelium. (F-H) Quantification of the marker-positive cells determined that PD0332991 (Cdk4/6 inhibitor) treatment induces differentiation while inhibiting proliferation in a dose-dependent manner. Reclustering analysis with TFs only (I) and expression patterns of the marker TFs (J). *Id* gene expression in the scRNA-seq data (K), PLISH for *Id2* (L), and quantification of *Id1*-, *2*-, and *3*-positive cells in PLISH (M) suggested that *Id* gene expression peaked at E14.5 and gradually decreased after that. (N) Double staining for Ki67 protein and *Id2* mRNA with immunostaining and PLISH suggested the dominant expression of Id2 in proliferating cells. * $p < 0.05$; Student's t test. ** $p < 0.05$; Tukey's test. Mean±SD, n=4–6 (C, M, N), 3 independent experiments (F, H). Scale bars: 5 μm (D, L, N), 10 μm (E, G).

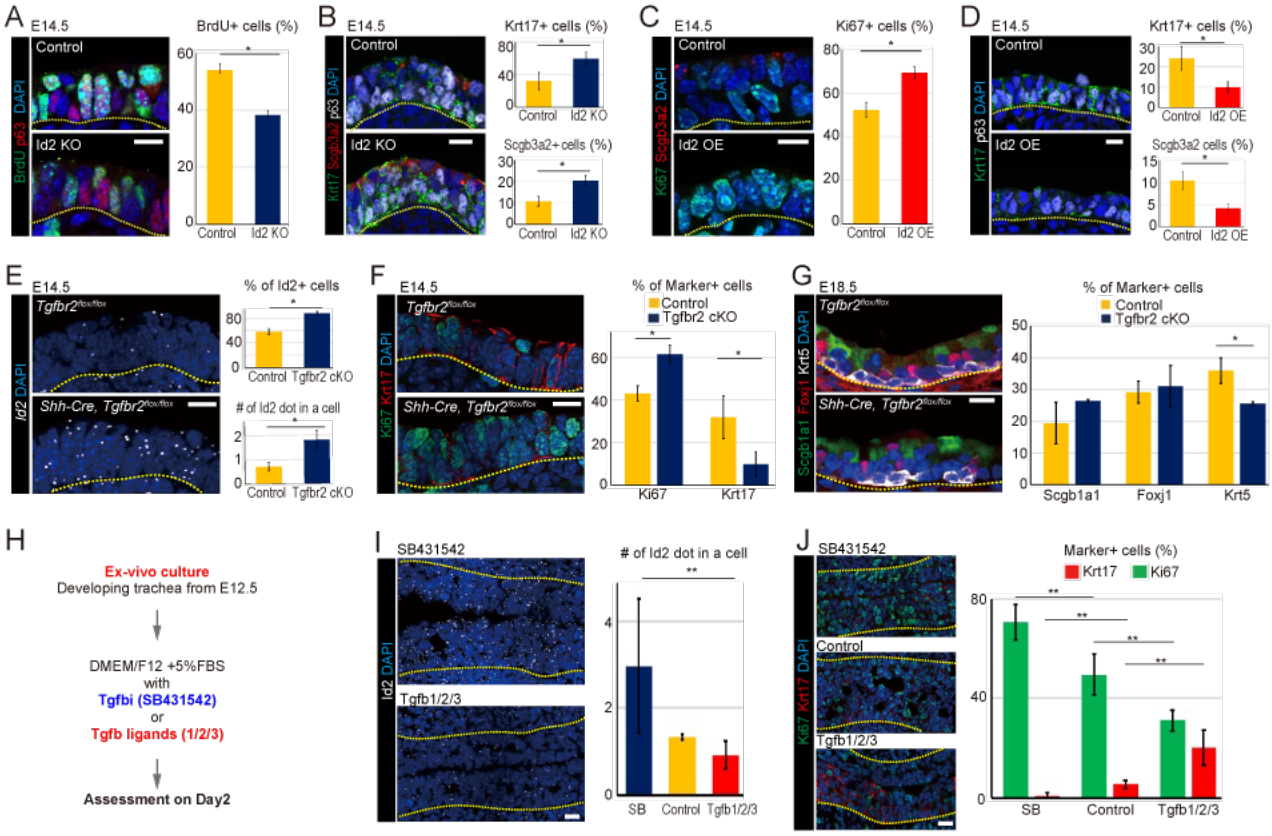

Figure 4. Tgfß signaling initiates cell cycle slowdown in epithelial cells by suppressing *Id2* gene expression.

The phenotypic analyses of tracheas from the *Id2* KO and OE groups assessed at E14.5 by immunostaining for BrdU and p63 (A), Scgb3a2 and Krt17 (B), Ki67 and Scgb3a2 (C), and p63 and Krt17(D) revealed that *Id2* promotes proliferation while inhibiting differentiation. (E) Differences in *Id2* expression between tracheas from the control and *Tgfbr2* KO groups assessed at E14.5 with PLISH confirmed that Tgfß signaling inhibits *Id2* expression. (F) Immunostaining for Ki67 and Krt17 in *Tgfbr2* KO epithelium at E14.5 showed that loss of Tgfß signaling suppresses Krt17 expression, enhancing proliferation. (G) At E18.5, epithelial *Tgfbr2* KO resulted in a significant decrease in mature basal cells but not in other cell types. (H) Schematic representation of *ex vivo* fetal trachea culture. Expression of *Id2* mRNA (PLISH) (I) and Ki67/Krt17 protein (immunostaining) (J) in *ex vivo* cultured trachea after 2 days of treatment with Tgfß-1/2/3 ligands or SB431542 confirmed that Tgfß signaling suppresses *Id2* and Ki67 expression, increasing Krt17 expression. * $p < 0.05$; Student's t test. ** $p < 0.05$; Tukey's test. Mean±SD, n=4-6 (A-G), 3 independent experiments (I- J). Scale bars: 5 µm.

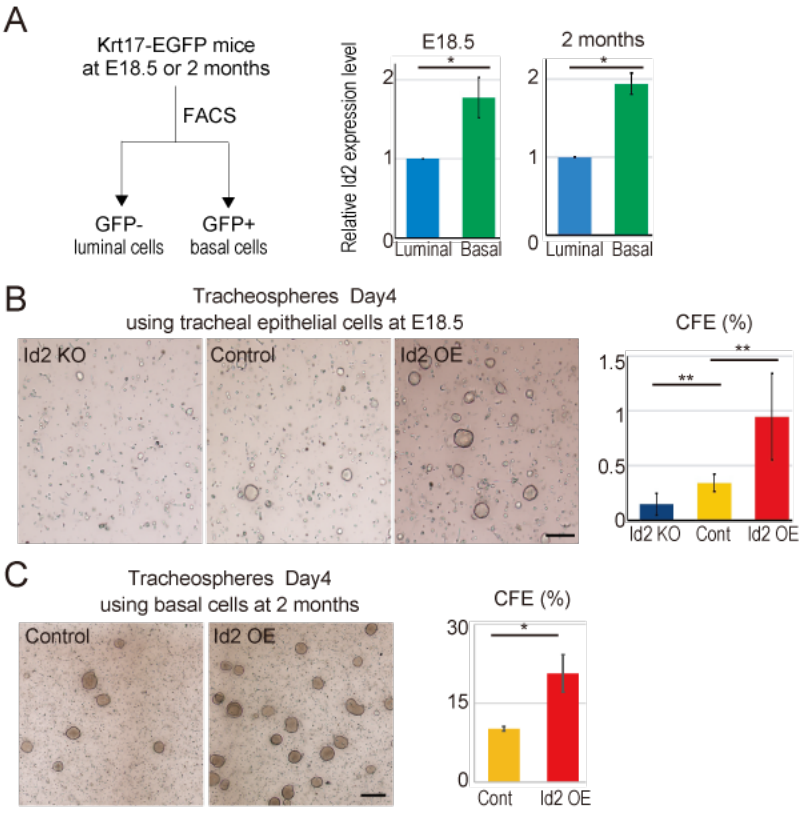

Figure 5. Predominant *Id2* expression in mature basal cells ensures their proliferative potential at perinatal and adult stages.

(A) Krt17^{+} and Krt17^{-} cells were sorted based on GFP intensity from the tracheas of Krt17-EGFP mice at E18.5 or 2 months, and *Id2* expression was assessed with qRT-PCR. *Id2* expression was significantly higher in the Krt17^{+} cells than in the Krt17^{-} cells at both timepoints. Tracheosphere culture at day 4 using tracheal epithelial cells derived from the *Id2* KO, control, and *Id2* OE mice at E18.5 (B) or 2 months (C) confirmed that the CFE reflects the dosage of *Id2* at both timepoints. * $p< 0.05$; Student's t test. ** $p< 0.05$; Tukey's test. Mean±SD, 4 independent experiments (A-C). Scale bars; 300 µm.

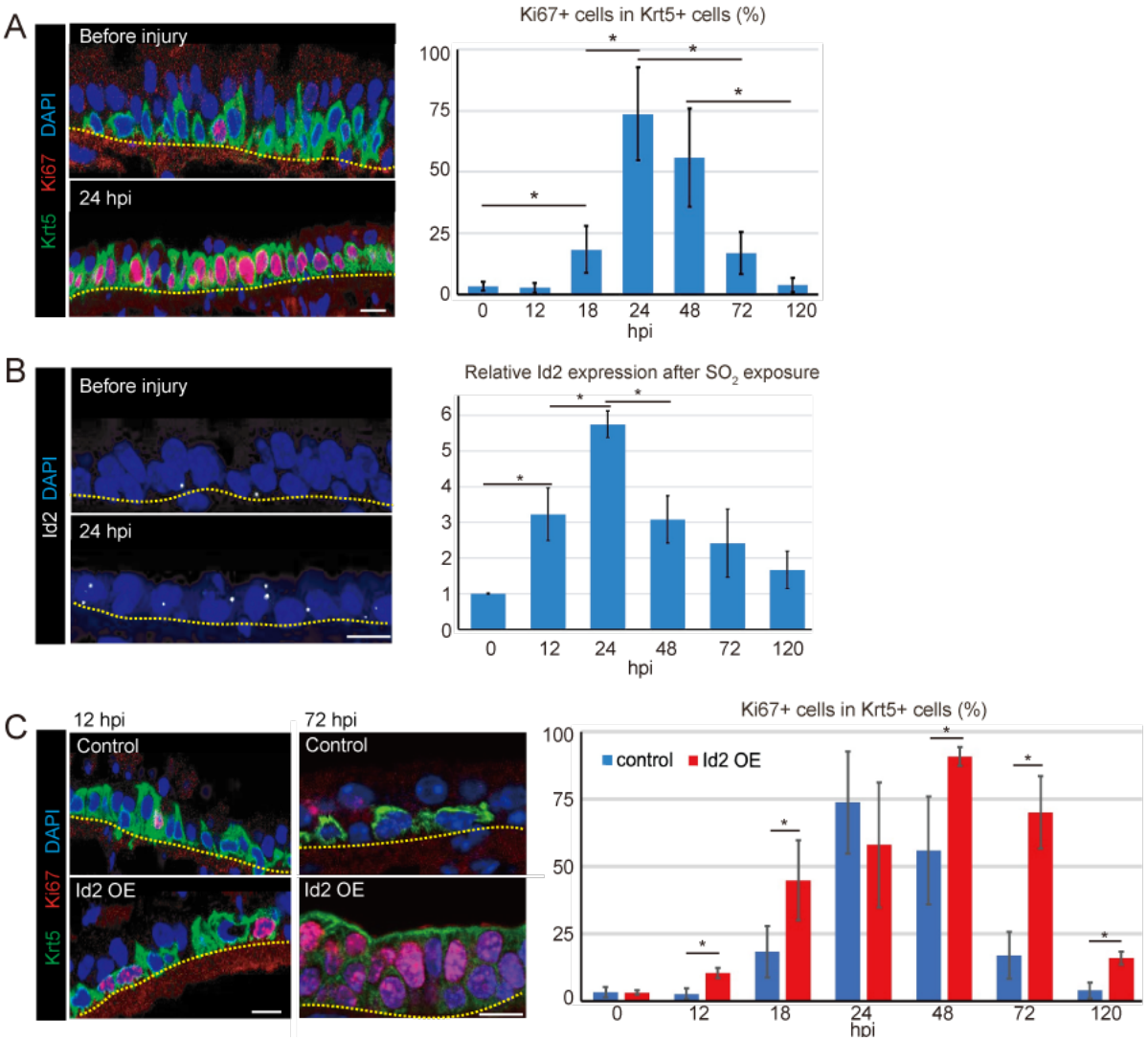

Figure 6. The slow-cycling basal cells re-enter the cell cycle with recurrent *Id2* activation following SO_2 injury.

(A) Assessment of proliferating basal cells in injured airway epithelium by immunostaining for Ki67 and Krt5. $Ki67^+$ proliferative cells in the $Krt5^+$ basal cell population started increasing at 18 hpi and peaked at 24 hpi in adult mice. (B) *Id2* expression during regeneration was assessed by PLISH. *Id2* expression started increasing at 12 hpi prior to the increase in $Ki67^+$ cells and peaked at 24 hpi. (C) Ki67 expression pattern assessed by immunostaining in the control and Id2 OE mice before or after SO_2 exposure confirmed that *Id2* dosage promotes basal cell self-renewal during the repair process. hpi, hours post injury. * $p < 0.05$; Tukey's test. Mean±SD, n=4-6 (A-C). Scale bars: 5 μm.

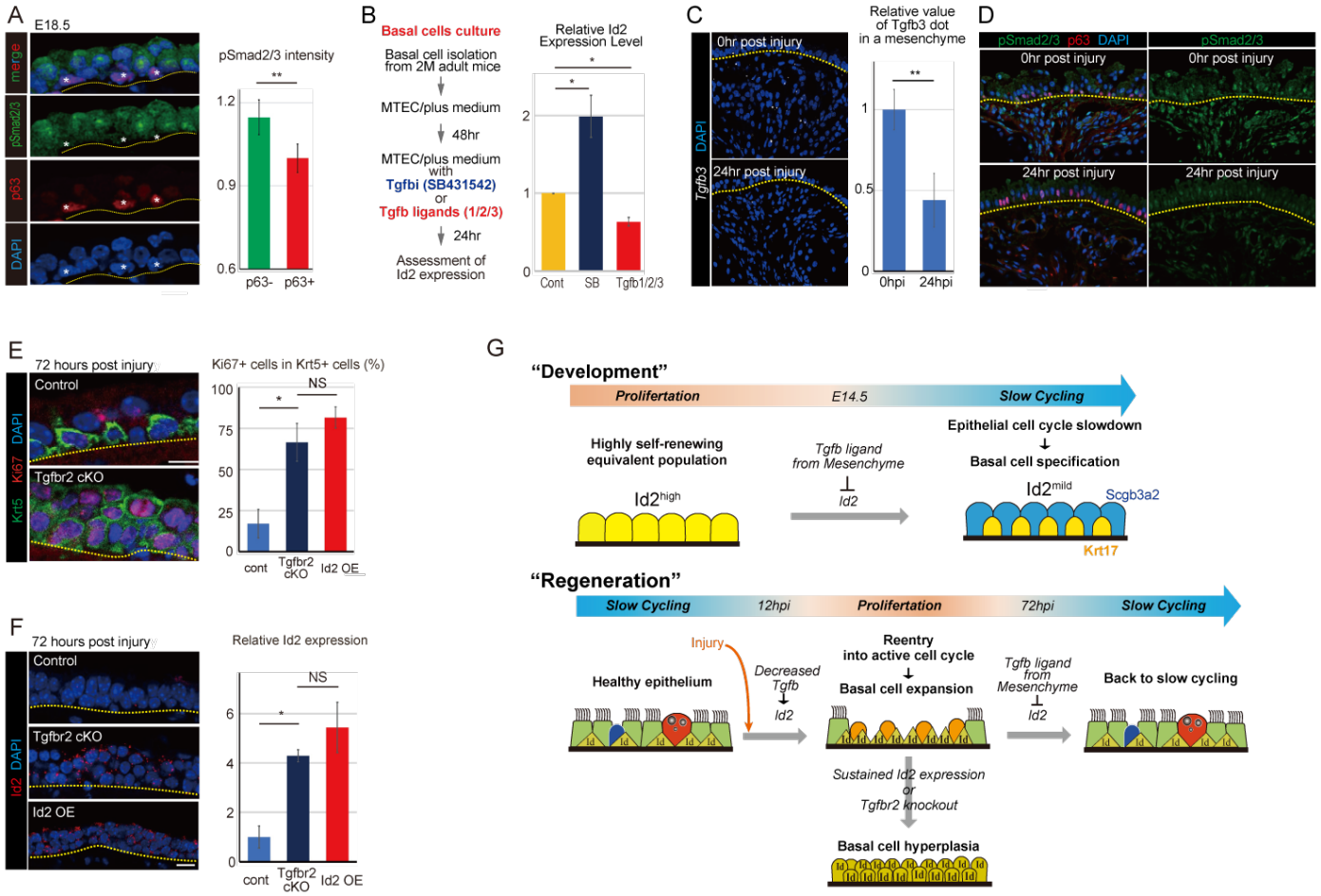

Figure 7. The inhibitory effect of Tgfβ signaling on *Id2* expression is conserved until adult stage.

(A) Quantitative assessment of pSmad2/3 staining intensity showed higher expression in the $p63^-$ luminal cells than in the $p63^+$ basal cells. Asterisks indicate the $p63^+$ basal cells. (B) Basal cells were sorted based on EpCAM/NGFR from the tracheas of 2-month-old wild-type mice, and *Id2* expression was assessed with qRT-PCR after 1 day culture with Tgfb ligands(1/2/3 or Tgfb inhibitor(SB431542). Tgfb inhibitor treatment significantly increased *Id2* expression, while Tgfb ligands treatment significantly decreased *Id2* expression. (C) *Tgfb3* detected by PLISH at 0 and 24 hpi confirmed the significant decrease of Tgfb3 expression in mesenchymal cells after SO_2 injury. (D) Immunostaining with anti-pSmad2/3 antibody demonstrated the decreased expression of pSmad2/3 in both epithelial and mesenchymal cells after SO_2 injury. (E) Assessment of proliferating basal cells in injured airway epithelium by immunostaining for Ki67 and Krt5. Tgfbr2 cKO mice phenocopied the basal cell hyperplasia phenotype seen in *Id2* OE mice. (F) *Id2* expression at 72hpi was assessed with RNAscope. *Id2* expression was significantly increased in *Tgfbr2* cKO and *Id2* OE mice compared to control. (G) Schematic summary of slow-cycling basal cell specification during development. *Id2* attenuation triggered by Mesenchymal-to-epithelial Tgfß signaling slows down the cell cycle and contributes to the specification of $Krt17^+$ basal cell progenitors. See discussion for the details. Schematic summary of the function of *Id2* gene during tissue regeneration following SO_2 injury. SO_2 injury decreases Tgfb3 secretion from mesenchyme, which reactivates *Id2* expression in basal cells. Recurrent *Id2* activation initiates basal cell expansion, but its sustained expression results in basal cell hyperplasia. See discussion for the details. hpi, hours post injury. * $p< 0.05$; Tukey's test. ** $p< 0.05$; Student's t test. NS; Not significant. Mean±SD, n=4-6 (A-C, E, F). Scale bars: 5 µm.

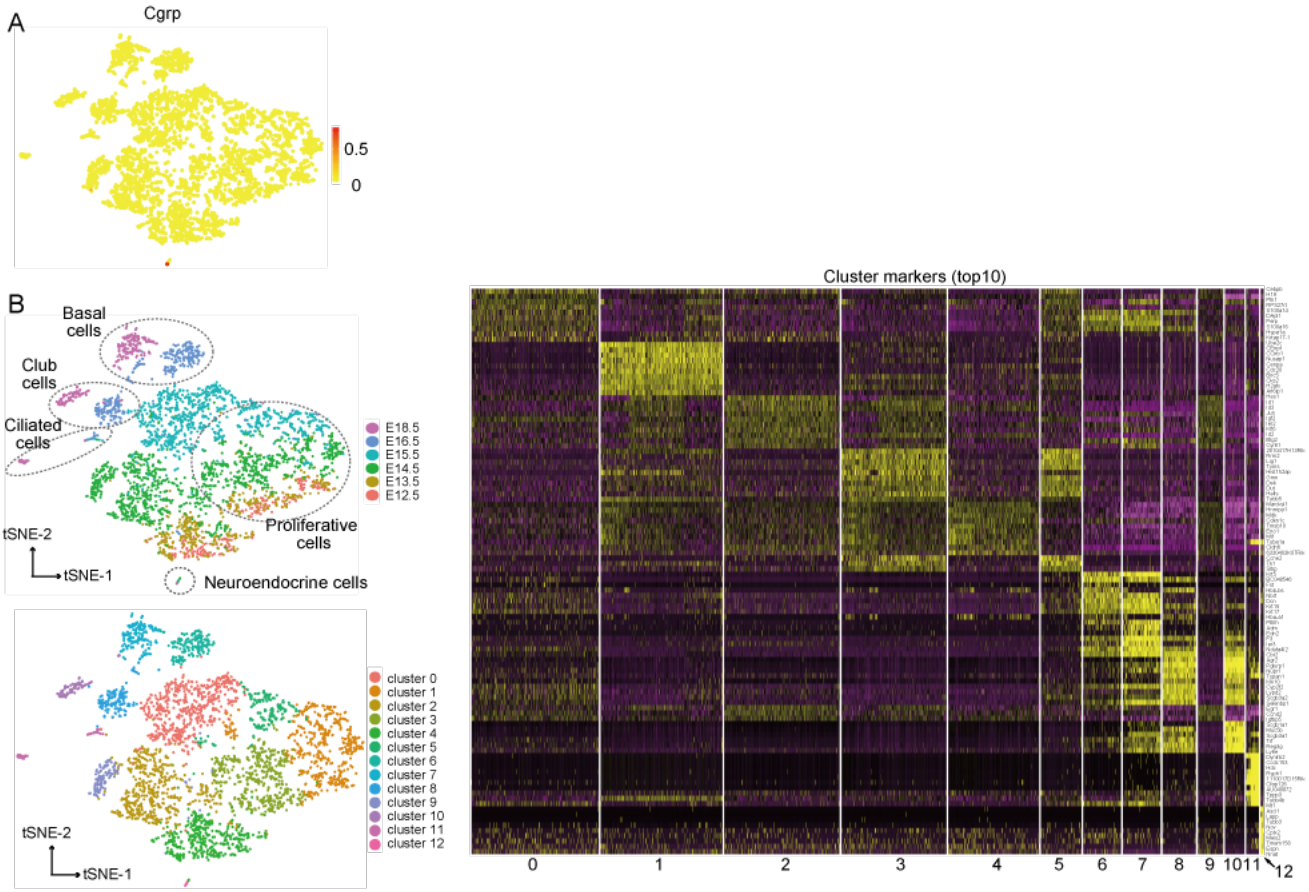

Figure S1. scRNA-seq analyses using embryonic progenitors

(A) Cgrp expression in the scRNA-seq dataset. (B) Clustering analysis and cluster markers (top 10) in a heatmap using embryonic progenitors from E12.5 to E18.5.

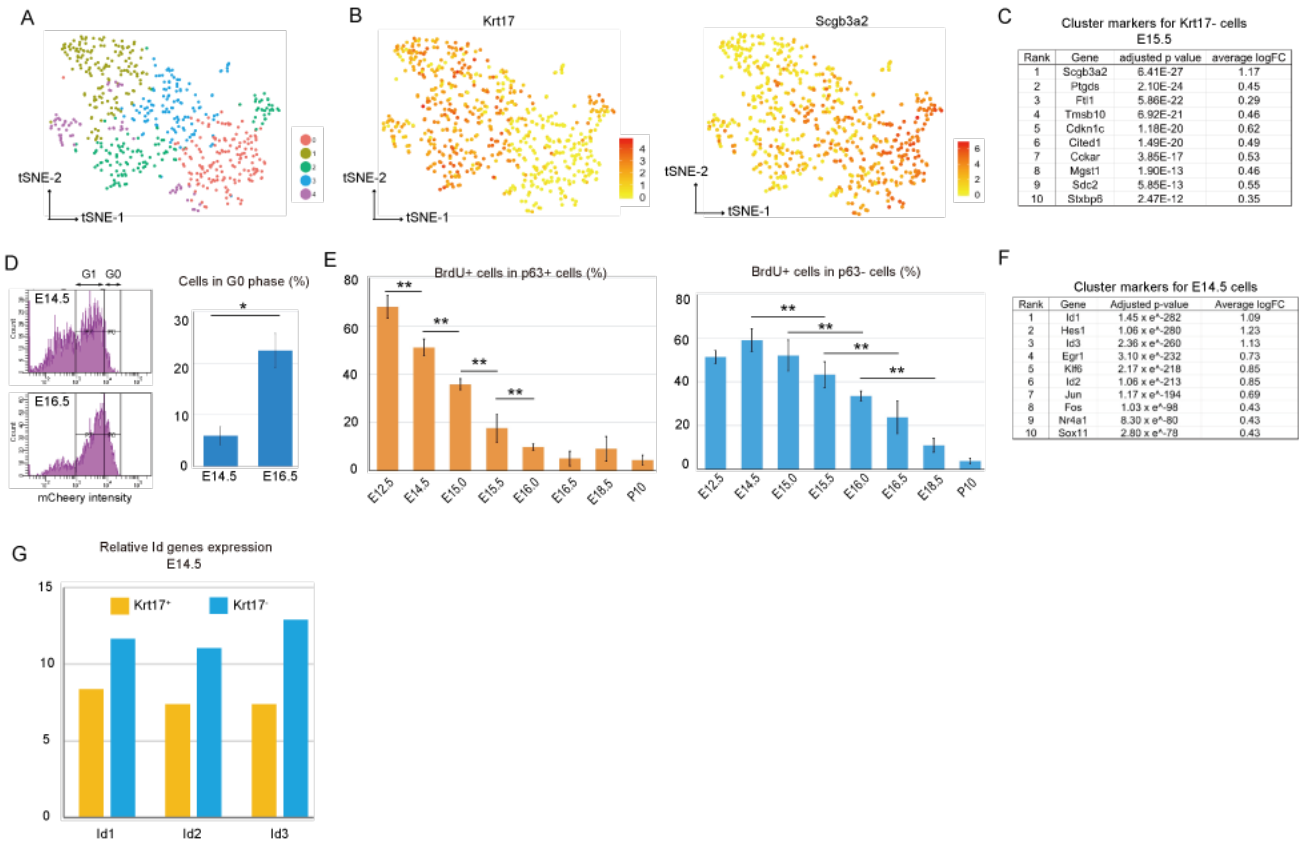

Figure S2. scRNA-seq analyses using E15.5 epithelial progenitors only and proliferative profile analyses

(A) Clustering analysis using epithelial cells from the E15.5 trachea only. (B) The mutually exclusive expression patterns of *Krt17* and *Scgb3a2* in E15.5 scRNA-seq data. (C) Top 10 cluster marker list for *Krt17*$^{-}$ cells at E15.5 based on the E15.5 scRNA-seq data. (D) The percentage of cells in G0 phase detected in Fucci mice (*Shh-Cre, Rosa*$^{H2B\text{-}EGFP/FucciG1}$) significantly increased at E16.5 compared with E14.5. (E) BrdU incorporation assay with immunostaining confirmed the earlier decline of BrdU^{+} proliferative cells in p63^{+} cell population than p63^{-} cell population. (F) Top10 cluster markers for the E14.5 cluster. (G) Id genes expression, which was calculated with E14.5 scRNA-seq dataset, was decreased in Krt17^{+} cells than Krt17^{-} cells at E14.5. * $p < 0.05$; Student's t test. ** $p < 0.05$; Tukey's test.

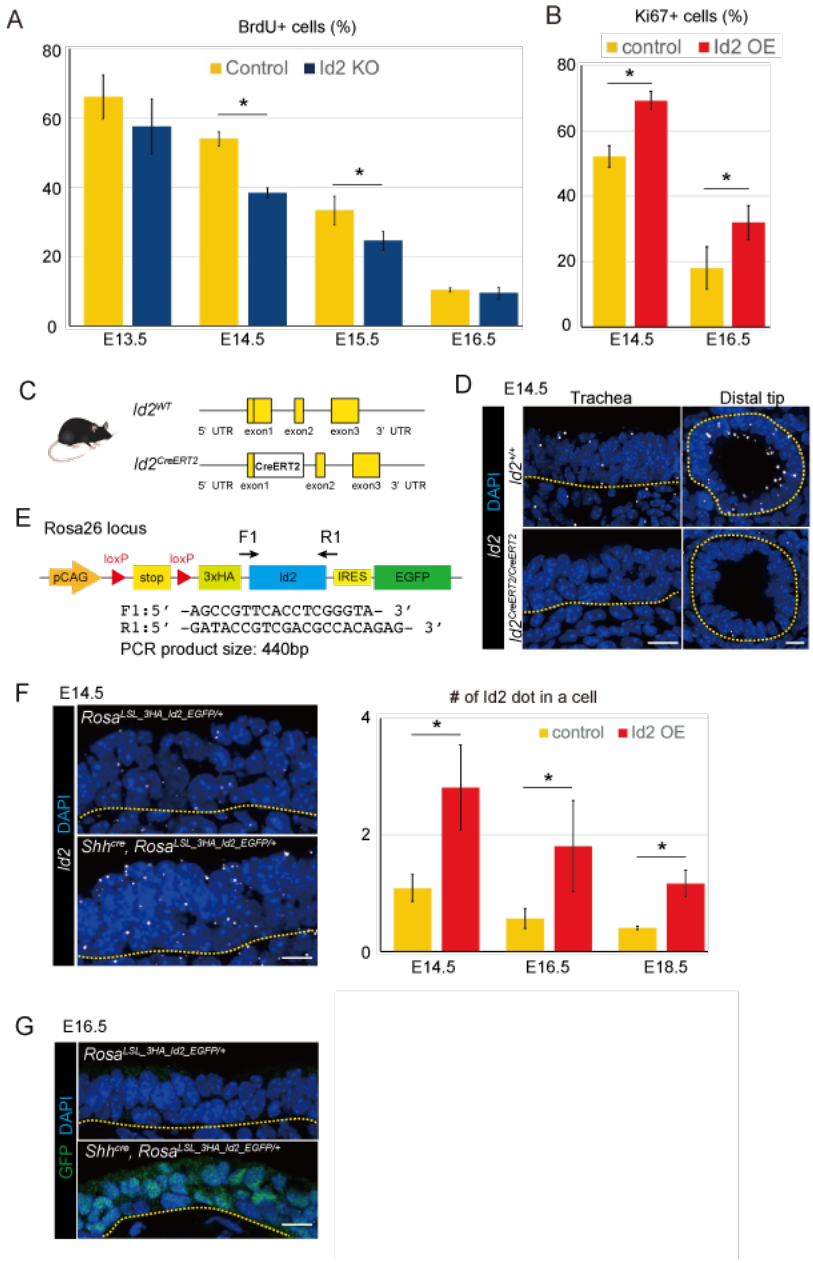

Figure S3. Phenotypes of *Id2* knockout and overexpression mice

(A) Time-series immunostaining analysis showed more BrdU^{+} epithelial cells in the *Id2*$^{+/+}$ mice (control) than the *Id2*$^{CreERT2/CreERT2}$ mice (*Id2* KO mice) at E14.5 and E15.5. (B) Time-series immunostaining analysis shows fewer Ki67^{+} epithelial cells in the *Rosa*$^{3xHA\text{-}Id2\text{-}IRES\text{-}H2B\text{-}EGFP}$ mice (control) than the *Shh*^{Cre}, *Rosa*$^{3xHA\text{-}Id2\text{-}IRES\text{-}H2B\text{-}EGFP}$ mice (*Id2* OE) at E14.5 and E16.5. (C) Schematic summary of the *Id2* locus in the wild-type and Id2$^{CreERT2/+}$ mice. (D) *Id2* expression detected by PLISH in the trachea and distal tip epithelium at E14.5 validates the knockout of *Id2* expression in the *Id2* KO mice. (E) Inserted construct in the Rosa26 locus of the *Rosa*$^{3xHA\text{-}Id2\text{-}IRES\text{-}H2B\text{-}EGFP}$ mice. (F) PLISH image analysis of *Id2* expression confirmed the overexpression of *Id2* in the *Id2* OE mice. (G) GFP detection with immunostaining at E16.5 in the control and *Id2* OE mice. * p< 0.05; Student's t test. Scale bars: 5 μm.

A

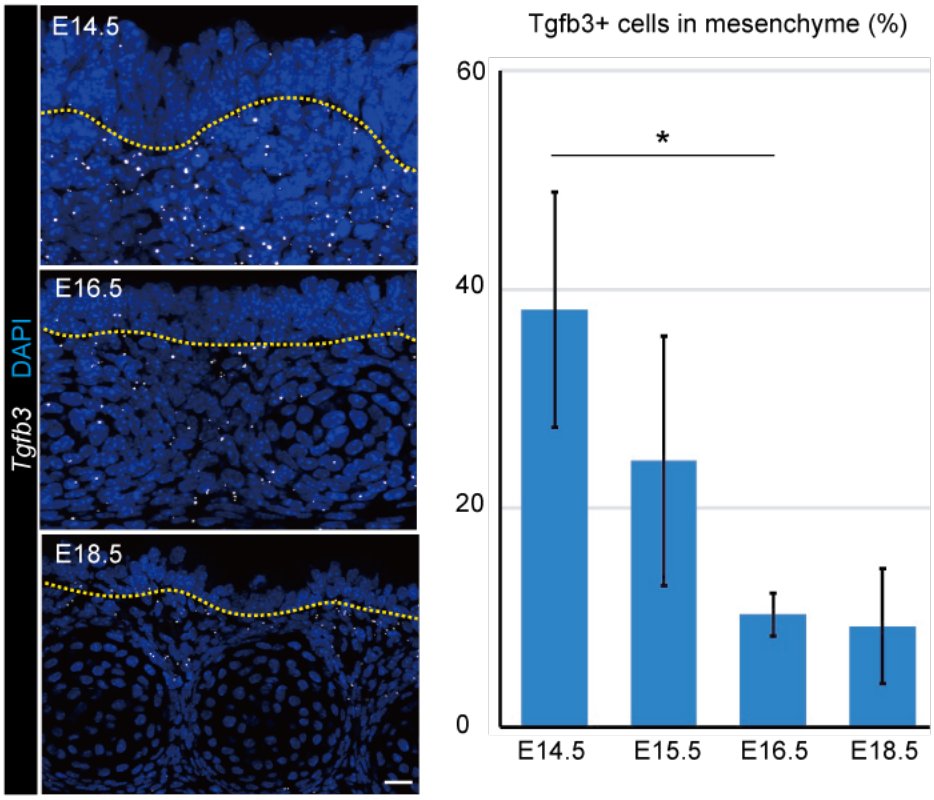

Figure S4. *Tgfb3* expression in the developing trachea

(A) *Tgfb3* detected by PLISH in the developing trachea from E14.5 to E18.5 confirmed that mesenchymal cells are the main source of Tgfb3 ligand during development, and their expression decreases over time.

* $p < 0.05$; Tukey's test. Scale bars: 10 μm.

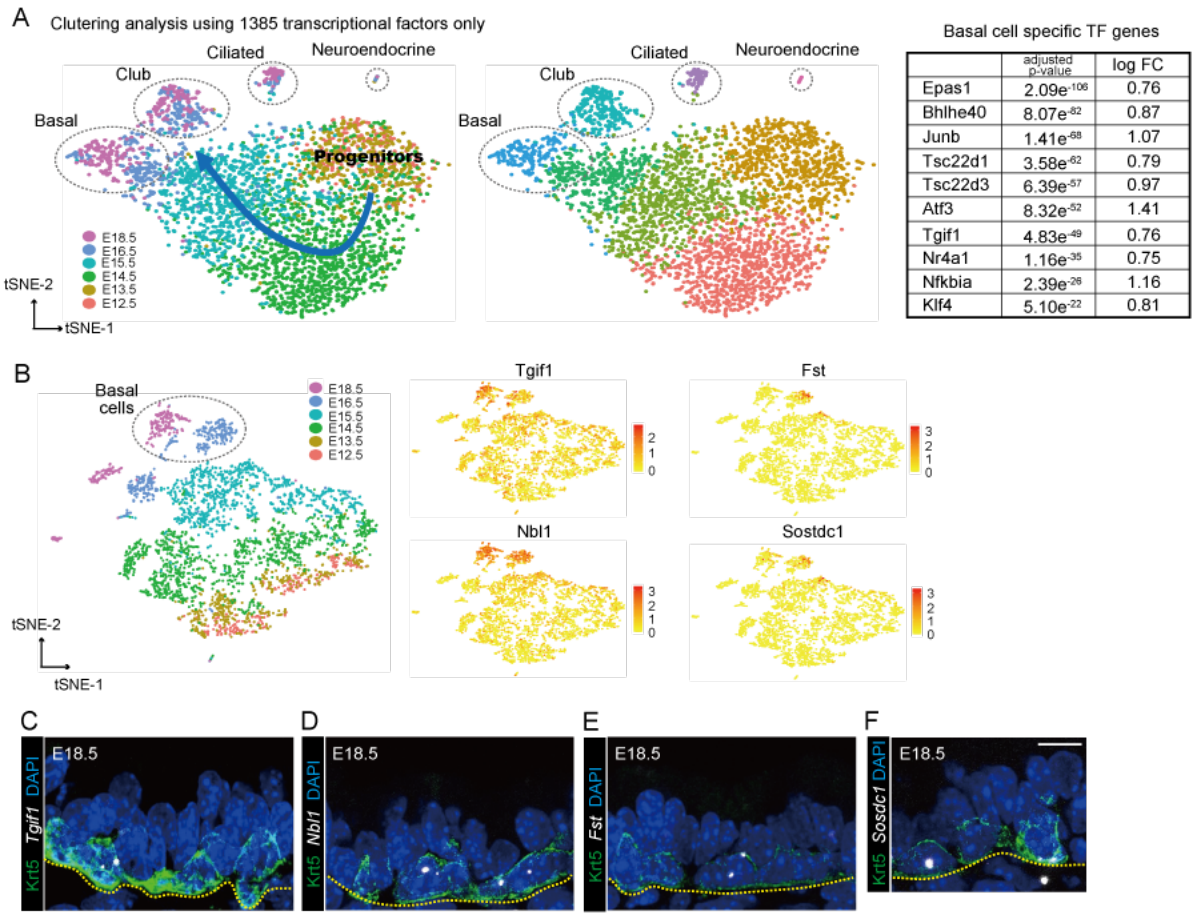

	adjusted p-value	log FC
Epas1	$2.09e^{-106}$	0.76
Bhlhe40	$8.07e^{-82}$	0.87
Junb	$1.41e^{-68}$	1.07
Tsc22d1	$3.58e^{-62}$	0.79
Tsc22d3	$6.39e^{-57}$	0.97
Atf3	$8.32e^{-52}$	1.41
Tgif1	$4.83e^{-49}$	0.76
Nr4a1	$1.16e^{-35}$	0.75
Nfkbia	$2.39e^{-26}$	1.16
Klf4	$5.10e^{-22}$	0.81

Figure S5. Basal cell lineage-specific genes detected in the scRNA-seq dataset

(A) The top 10 list of basal cell-specific transcription factors (TFs) detected by clustering analysis using TFs only. (B) The expression of 4 genes (*Tgif1*, *Nbl1*, *Fst*, and *Stdc1*) in the t-SNE map that are specifically expressed in basal cells in the later stage of development. The spatial expression patterns of *Tgif1* (C), *Nbl1* (D), *Fst* (E), and *Stdc1* (F) detected by PLISH. Scale bars: 5 μm.

STAR★METODS

Detailed methods are provided in the online version of this paper and include the following:

- ●KEY RESOURCES TABLE
- ●LEAD CONTACT AND MATERIALS AVAILABILITY
- ●EXPERIMENTAL MODEL
  - ○MICE
- ●METHOD DETAILS
  - ○BrdU-incorporation assay
  - ○Cell cycle analysis
  - ○Cell dissociation and FACS
  - ○Ex-vivo trachea culture experiment
  - ○Microscopy and imaging
  - ○Immunohistochemistry
  - ○Quantitative RT-PCR (qPCR)

16 ○Single cell RNA-seq for sequencing library construction

17 ○Single cell RNA-seq analyses

18 ○Single molecule in-situ hybridization (PLISH)

19 ○Single molecule in-situ hybridization (RNAscope)

20 ○SO_2 airway injury model

21 ●QUANTIFICATION AND STATISTICAL ANALYSIS

22 ○Statistical analysis

23 ●DATA AND CORE AVAILABILITY

24 ○Antibodies

25 ○Chemicals, Peptides, and Recombinant Proteins

26 ○Critical Commercial Assays

27 ○Deposited Data

28 ○Experimental Models: Organisms/Strains

29 ○Oligonucleotides

30 ○Software and Algorithms

31 **KEY RESOURCES TABLE**

REAGENT or RESOURCE	SOURCE	IDENTIFIER
Antibodies		
Chicken anti-GFP	Thermo Fisher Scientific	Cat# A10262, RRID:AB_2534023
Goat anti-Scgb1a1	Santa Cruz	Cat# sc-9772, RRID:AB_2238819
Mouse anti-Foxj1	eBioscience	Cat# 14-9965-82, RRID:AB_1548835
Mouse anti-Ki67	BD Biosciences	Cat# 550609, RRID:AB_393778
Mouse anti-Krt17	Santa Cruz	Cat# sc-393002, RRID: N/A
Mouse anti-p63	Abcam	Cat# ab735, RRID:AB_305870
Rabbit anti-GFP	MBL international	Cat# 598, RRID:AB_2313843
Rabbit anti-Krt17	Abcam	Cat# ab53707, RRID:AB_869865
Rabbit anti-Krt5	Abcam	Cat# ab24647, RRID:AB_448212
Rabbit anti-pSmad2/3	Cell Signaling	Cat# 8828, RRID:AB_2631089
Rabbit anti-p75 NGF Receptor	Abcam	Cat# ab8875 RRID:AB_306828
Rabbit anti-Scgb3a2	Dr. Shioko Kimura's lab	https://ccr.cancer.gov/Laboratory-of-Metabolism/shioko-kimura
Rat anti-BrdU	Abcam	Cat# ab6326, RRID:AB_2313786
Alexa Fluor 488 Donkey anti-rabbit	Life Technology	Cat# A-21206, RRID:AB_141708
Alexa Fluor 488 Donkey anti-rat	Life Technology	Cat# A-21208, RRID:AB_141709
Alexa Fluor 488 Goat anti-chicken	Life Technology	Cat# A-11039, RRID:AB_142924
Alexa Fluor 594 Donkey anti-goat	Life Technology	Cat# A-11058, RRID:AB_142540
Alexa Fluor 594 Donkey anti-mouse	Life Technology	Cat# A-21203, RRID:AB_141633
Alexa Fluor 594 Donkey anti-rabbit	Life Technology	Cat# A-21207, RRID:AB_141637
Alexa Fluor 647 Donkey anti-mouse	Life Technology	Cat# A-31571, RRID:AB_162542
Alexa Fluor 647 Donkey anti-rabbit	Life Technology	Cat# A-31573, RRID:AB_2536183
anti-EpCAM, APC	Invitrogen	Cat# 17-5791-80, RRID:AB_2734965

APC Rat IgF2a, Isotype Ctrl Antibody	BioLegend	Cat# 400511, RRID: N/A
BSI-B4, FITC conjugate	Sigma-Aldrich	Cat# L2895 RRID: N/A
Chemicals, Peptides, and Recombinant Proteins		
Collagenase Type Ⅰ	Worthington Biochemical Corporation	Cat# CLS1
5-Bromo-2′-deoxyuridine	Sigma-Aldrich	Cat# B5002
apo-Transferrin human powder	Sigma-Aldrich	Cat# T1147
Bovine Pituitary Extract (BPE)	Thermo Fisher Scientific	Cat# 13028014
Can Get Signal ® immunostain Solution B	Toyobo life science	Cat# NKB-601
Cholera toxin	Wako	Cat# 030-16331
Corning® Collagen type Ⅰ	Corning	Cat# 354236
Corning® Epidermal Growth Factor (EGF)	Corning	Cat# 354001
Corning® Matrigel® Growth Factor Reduced (GFR) Basement Membrane Matrix	Corning	Cat# 354230
DAPI	Nacalai	Cat# 11034-56
Deoxyribonuclease I	Sigma-Aldrich	Cat# DN25
DEPC treated-Water	Nacalai	Cat# 36415-54
Dispase	Corning	Cat#354235
DMEM/Ham's F-12	Nacalai	Cat# 11582-05
DMEM/Ham's F-12 50/50 Mix	Corning	Cat# 15-090-CVR
dNTP Mix	Invitrogen	Cat# 18427013
EDTA (0.5M, pH 8.0)	Nippon gene	Cat# 311-90075
Fetal Bovine Serum	Sigma-Aldrich	Cat# F7524
Fluoromount™	Diagnostic BioSystems	Cat# K024
Formamide	Nacalai	Cat# 16345-65
Glycerol	Nacalai	Cat# 17045-94
Heparin sodium salt	Sigma-Aldrich	Cat# H3393
HEPES	Nacalai	Cat# 17514-86
HistoVT One	Nacalai	Cat# 06380
InSolution™ γ-Secretase Inhibitor IX	Sigma-Aldrich	Cat# 565784
Insulin from bovine pancreas powder	Sigma-Aldrich	Cat# I6634
NxGen® phi29 DNA Polymerase	Lucigen	Cat# 30221
PD00332991, Cdk4/Cdk6 inhibitor	Abcam	Cat# ab218118
Penicillin-Streptomycin Mixed Solution	Nacalai	Cat# 09367-34
Random Primers	Invitrogen	Cat# 48190011
RBC Lysis Buffer (10X)	BioLegend	Cat# BL420301
Recombinant Human TGF-beta 1	R&D systems	Cat# 240-B
Recombinant Human TGF-beta 2	R&D systems	Cat# 302-B2
Recombinant Human TGF-beta 3	R&D systems	Cat# 243-B3
RNAscope® Probe - Mm-Id2	Advanced Cell Diagnostics	Cat# 445871
RNAscope(R) Multiplex Fluorescent Reagent Kit v2	Advanced Cell Diagnostics	Cat# 323100
RNaseOUT™ Recombinant Ribonuclease Inhibitor	Thermo Fisher Scientific	Cat# 10777019
Sodium Chloride	Nacalai	Cat# 31333-45
Sodium trichloroacetate	Sigma-Aldrich	Cat# 190780
SuperScript™ III Reverse Transcriptase	Invitrogen	Cat# 18080

T4 DNA Ligase	New England BioLabs	Cat# M0202T
Tamoxifen	Sigma-Aldrich	Cat# T5648
TGF-β RI Kinase Inhibitor VI, SB431542	Sigma-Aldrich	Cat# 616461
THUNDERBIRD® SYBR qPCR Mix	Toyobo life science	Cat# QPS-201
Tris(hydroxymethyl)aminomethane	Nacalai	Cat# 35434-21
Trisodium Citrate Dihydrate	Fujifilm	Cat# 204-16675
TRIzol™ Reagent	Invitrogen	Cat# 15596018
Trypsin-EDTA (0.25%), phenol red	Thermo Fisher Scientific	Cat# 25200056
Tween®20	Nacalai	Cat# 28353-85
UltraPure™ BSA	Invitrogen	Cat# AM2616
Y-27632, Dihydrochloride Salt	LC laboratories	Cat# Y-5301
Critical Commercial Assays		
Chromium Single Cell 3' Library & Gel Bead Kit v2	10X Genomics	Cat# PN-120237
Direct-zol RNA MicroPrep	Zymo research	Cat# R2060
RNeasy Mini Kit	Qiagen	Cat# 74104
SPRIselect Reagent Kit	Beckman Coulter	Cat# B23318
VECTOR M.O.M. Immunodetection Kit	Vector laboratories	Cat# VEC-BMK-2202-1
Deposited Data		
scRNA-seq datasets	This paper	GSE152692
Experimental Models: Organisms/Strains		
Mouse: Shh^{Cre}	Harfe BD et al. Cell. 2004.	JAX Stock No: 005622
Mouse: $Krt17^{CreERT2}$	Doucet et al. Cell Rep. 2013.	N/A
Mouse: $Id2^{CreERT2}$	Rawlins EL et al. Development. 2009.	JAX Stock No: 016222
Mouse: $Rosa26^{mTmG}$	Muzumdar MD et al. Genesis. 2007.	JAX Stock No: 007676
Mouse: $Rosa26^{FucciG1}$	Abe T et al. Development. 2013.	N/A
Mouse: $Krt17^{EGFP}$	Bianchi N et al. Mol Cell Biol. 2005	JAX Stock No: 023965
Mouse: N2IP::Cre	Liu Z et al. Dev. Cell 2013	N/A
Mouse: $Rosa26^{LSL\text{-}Id2\text{-}IRES\text{-}H2B\text{-}EGFP}$	This paper	N/A
Mouse: $RBPj^{flox/flox}$	Tanigaki K et al. Nat Immunol. 2002.	N/A
Mouse: $Rosa26^{Ai3}$	Madisen L et al. Nat Neurosci. 2010.	JAX Stock No: 007903
Mouse: $Tgfbr2^{flox/flox}$	Leveen P et al. Blood. 2002.	JAX Stock No: 012603
Oligonucleotides		
Gapdh for qPCR	AATGTGTCCGTCGTGGATCTGA	GATGCCTGCTTCACCACCTTCT
Id2 for qPCR	GCCCAGGTGTCGTTCTCCG	TTCCAACTGTAGAAAGGGCACTG
Common Bridge for PLISH	5' TCAACTCGACGTATAACATAACGACGTAAGT 3'	

Connector Circle for PLISH	5' TGTTAGCGCTAACAAAATGCTGCT GCTGTACTACGAACAACAATACAC ATGTTACGACGT 3'	
Cy5-DP5 for PLISH	5' Cy5 AATGCTGCTGCTGTACTACGG 3'	
Fst (Right probe) for PLISH	5' CATGGCACACTCGCTGGCGTTTAT ACGTCGAGTTGAACGTCGTAACA 3'	
Fst (Left probe) for PLISH	5' TAGCGCTAACAACTTACGTCGTTA TGATGTGGCATTGTCACTGGCA 3'	
Id1 (Right probe) for PLISH	5' AACCCCCTCCCCAAAGTCTCTTAT ACGTCGAGTTGAACGTCGTAACA 3'	
Id1 (Left probe) for PLISH	5' TAGCGCTAACAACTTACGTCGTTA TGTGGAGGCTGAAAGGTGGAGA 3'	
Id2 (Right probe) for PLISH	5' GTCGTCCACCGGGGTTTTGCTTAT ACGTCGAGTTGAACGTCGTAACA 3'	
Id2 (Left probe) for PLISH	5' TAGCGCTAACAACTTACGTCGTTA TGTCCGGGAGATGCCCAAGCTG 3'	
Id3 (Right probe) for PLISH	5' CATTCTCGGAAAAGCCAGTCTTAT ACGTCGAGTTGAACGTCGTAACA 3'	
Id3 (Left probe) for PLISH	5' TAGCGCTAACAACTTACGTCGTTA TGTTTTAGACTTGAGTCAGGGT 3'	
Nbl1 (Right probe) for PLISH	5' TGGGACTGGAGCTTCCGACCTTA TACGTCGAGTTGAACGTCGTAACA 3'	
Nbl1 (Left probe) for PLISH	5' TAGCGCTAACAACTTACGTCGTTA TGTCTGCAAGCGGTCTTCCCAC 3'	
Sostdc1 (Right probe) for PLISH	5' GGATCCTCTGGGTGCGCGTCTTA TACGTCGAGTTGAACGTCGTAACA 3'	
Sostdc1 (Left probe) for PLISH	5' TAGCGCTAACAACTTACGTCGTTA TGTTGTCGTTGACACACCGCCA 3'	
Tgfb3 (Right probe) for PLISH	5' AGAAGTTGGCATAGTAACCCTTAT ACGTCGAGTTGAACGTCGTAACA 3'	
Tgfb3 (Left probe) for PLISH	5' TAGCGCTAACAACTTACGTCGTTA TGTTAGGTTCGTGGACCCATTT 3'	
Tgif1 (Right probe) for PLISH	5' CTGTAAAGTTGCTGGGTGCTTTAT ACGTCGAGTTGAACGTCGTAACA 3'	
Tgif1 (Left probe) for PLISH	5' TAGCGCTAACAACTTACGTCGTTA TGATTTGCGGTACATCTGTACT 3'	

Software and Algorithms		
Cellranger v2.2.0	10x genomics	https://www.10xgenomics.com/solutions/single-cell/
CellSens Dimension2.1		Olymp
ImageJ	NIH	https://imagej.net/NIH_Image
Monocle v2.8.0	Github	http://cole-trapnell-lab.github.io/monocle-release/docs/
Seurat v2.3.4	Satija Lab	https://satijalab.org/seurat/
ZEN2012	Carl Zeiss	https://www.zeiss.com/microscopy/int/products/microscope-software/zen.html

LEAD CONTACT AND MATERIALS AVAILABILITY

Further information and requests for resources and reagents should be directed to and will be fulfilled by the Lead Contact, Dr. Mitsuru Morimoto (mitsuru.morimoto@riken.jp). This study did not generate new unique reagents.

EXPERIMENTAL MODEL

MICE

The Institutional Animal Care and Use Committee of RIKEN Kobe Branch approved all

the experimental procedures using animal in accordance with the ethics guidelines of the institute. All mouse strains were maintained in the RIKEN BDR animal facility in specific pathogen free (SPF) conditions.

See **KEY RESOURCES TABLE** for information of each mice line. To minimalize tissue deformation, in all experiments, embryos were fixed in 4% paraformaldehyde/phosphate buffered saline (PBS) overnight at 4 °C or 3 hours at room temperature, and then tracheas were dissected.

Generation of *Rosa*$^{CAG\text{-}LSL\text{-}3xHA\text{-}Id2\text{-}IRES\text{-}H2B\text{-}EGFP/+}$ mice line

To generate a knock-in mouse expressing 3xHA-Id2 and H2B-EGFP that was conditionally incorporated into the ROSA26 locus, Gt(ROAS)26Sor$^{tm1CAG\text{-}LSL\text{-}3xHA\text{-}Id2\text{-}IRES\text{-}H2B\text{-}EGFP}$ (Accession No. CDB0076E: http://www2.clst.riken.jp/arg/mutant%20mice%20list.html) mouse (Figure S3E), was established with CRISPR/Cas9 genome editing technology in zygotes as described previously(Abe, et al., 2020). In brief, the ROSA26 donor vector was constructed using Gateway technology (Thermo Fisher Scientific). The Gateway destination vector, named pR26-CAG-STOP-HR-DEST, was modified from pBigT(Srinivas, et al., 2001), pCAGGS(Niwa, et al., 1991), R26-H2B-EGFP HR donor vector(Abe, et al., 2020).

pENTR2B-3xHA-Id2-IRES-H2B-EGFP was recloned into the destination vector using LR clonase of the Gateway technology in order to generate the donor vector. The donor vector was injected into C57BL/6 zygotes and the knock-in F0 mice were identified by PCR(Abe, et al., 2020). Genotype was determined by genetic PCR with combination of following primers; F1: 5'- AGCCGTTCACCTCGGGTA-3', R1: 5'-GATACCGTCGACGCCACAGAG-3' (440bp).

METHOD DETAILS

BrdU-incorporation assay

To label almost all of proliferating cells, BrdU (0.1 mg ml^{-1}, Sigma-Aldrich, B5002) were cumulatively injected into pregnant mice four times every 2 h before sacrifice. To measure the proliferating ratio, $BrdU^+$ cells were manually counted in the ventral epithelium between the 1st and 12th cartilage region, based on the sections immunostained for BrdU. Before E13.5, when the cartilage did not appear yet, the cells were counted in the entire region of the trachea in sagittal sections.

Cell cycle analysis

For the assessment of cell cycle status in epithelial cells in developing trachea at E14.5

and E16.5, $Rosa^{FucciG1/+}$ mice (Abe, et al., 2013) were mated with Shh^{Cre}, $Rosa^{H2B\text{-}EGFP/+}$. The developing trachea dissected from Shh^{Cre}, $Rosa^{H2B\text{-}EGFP/FucciG1}$ were digested by 0.25% Trypsin (Thermo Fisher Scientific, 25200056), 0.5mg/ml DNase Ⅰ (Sigma-Aldrich, DN25), and 1x RBC lysis buffer (BioLegend, BL420301). The single cell suspension was obtained after passing cells through a 40 mm cell strainer. Then, the single cell suspension was sorted for selecting GFP+ epithelial cells using BD FACS Aria II appliance. Based on mCherry intensity, GFP+ epithelial cells were classified into three population such as $mCherry^{negative}$, $mCherry^{moderate}$, and $mCherry^{high}$ cells. We defined that $Cherry^{moderate}$ and $mCherry^{high}$ cells are in G1 and G0 phases respectively in accordance with the previous paper (Abe, et al., 2013).

Cell dissociation and FACS

To collect $Krt17^{+}$ and $Krt17^{-}$ cells using $Krt17^{EGFP}$ mice at E18.5, single-cell suspensions were made through the incubation of trachea with Trypsin-EDTA (0.25%) (Thermo Fisher Scientific, 25200056) at 37℃ for 60 min, followed by gentle pipetting and passage through a 40 mm cell strainer. For FACS with EpCAM-APC (Invitrogen, 17-5791-80), cells were diluted to less than 1 $\times 10^6$ cells/mL in PBS with 3% FBS and incubated in 1:100 EpCAM-APC (Invitrogen, 17-5791-80) or 1:100 IgG-APC isotype control (BioLegend, 400511) on ice for 30 min, followed by PBS wash. Sorting was performed

93 on BD FACS Aria II and data analyzed with FACS Diva (BD Biosciences). Cells were
94 collected in MTEC/Plus and cultured immediately or frozen for RNA extraction.

95 To prepare single-cell suspensions from adult trachea, the epithelial sheet was peeled off
96 from mesenchymal tissue in trachea with a tungsten needle after the incubation with
97 400U/ml collagenase type Ⅰ (Worthington Biochemical Corporation, CLS1) at 37℃ for
98 60 min or 16U/ml Dispase (Corning) at 37℃ for 40 min. Single-cell suspensions were
99 made through the incubation with Trypsin-EDTA (0.25%) at 37℃ for 60 min, followed
100 by gentle pipetting, passage through a 40 mm cell strainer, and incubation in 1x RBC
101 lysis at RT for 3 min. For FACS with EpCAM-APC, cells were diluted to less than 1×10^6
102 cells/mL in PBS with 3% FBS and incubated in 1:100 EpCAM-APC or 1:100 IgG-APC
103 isotype control on ice for 30 min, followed by PBS wash. Sorting was performed on BD
104 FACS Aria II and data analyzed with FACS Diva. Cells were collected in MTEC/Plus and
105 cultured immediately or frozen for RNA extraction.

106 Single-cell suspensions at E18.5 and 2M for tracheosphere culture were made through
107 the incubation of trachea with Trypsin-EDTA (0.25%) (Thermo Fisher Scientific,
108 25200056) at 37℃ for 30-60 min, followed by gentle pipetting and passage through a 40
109 mm cell strainer. To remove the mesenchymal cells, all the cells were incubated at 37℃
110 for 2 hours in DMEM/Ham's F-12 (Nacalai, 11582-05) with 5% FBS. Floating cells were

111 collected and used as epithelial cells for the further tracheosphere culture. The day when
112 culture experiment started was defined as day0. 500µl MTEC/Plus was added to each
113 well and changed at Day1, 3. 10µM Y-27632 (LC laboratories, Y-5301) was
114 supplemented at Day0 and Day1 only. The number of spheres with the diameter over
115 50µm per well was counted on Day4 using an inverted microscope.

116 To isolate basal cells at 2M for tracheosphere or two-dimensional culture, the epithelial
117 sheet was peeled off from mesenchymal tissue in trachea with a tungsten needle after the
118 incubation with 16U/ml Dispase (Corning) at 37℃ for 40 min. Single-cell suspensions
119 were made through the incubation with Trypsin-EDTA (0.25%) at 37℃ for 20 min,
120 followed by gentle pipetting, passage through a 40 mm cell strainer. For FACS, cells were
121 diluted to less than 1×10^6 cells/mL in PBS with 3% FBS and incubated in 1:100 EpCAM-
122 APC and 1:200 anti-p75 NGF receptor antibody or 1:100 anti-BSI B_4-FITC antibody on
123 ice for 30 min, followed by PBS wash. In the case of anti-p75 NGF receptor antibody
124 staining, incubation with 1:500 Alexa Fluor 488 Donkey anti-rabbit on ice for 30 min was
125 followed. Sorting was performed on BD FACS Aria II and data analyzed with FACS Diva.
126 Cells were collected in MTEC/Plus and cultured immediately. For tracheosphere culture,
127 2×10^3 basal cells were co-cultured with 4×10^4 fibroblast cells in 25ul Growth-factor
128 reduced Matrigel with 75ul MTEC/Plus (total 100ul/well). 500µl MTEC/Plus was added

to each well and changed at Day1, 3. 10μM Y-27632 (LC laboratories, Y-5301) was supplemented at Day0 and Day1 only. The number of spheres with the diameter over 50μm per well was counted on Day4 using an inverted microscope. For two-dimensional culture, 1.5×10^4 basal cells in 300ul MTEC/Plus were seeded onto 24-well 0.4-μm Transwell insert (Corning, #3470) coated with collagen type Ⅰ (Corning, 354236). 0.5mL MTEC/Plus was added to the lower chamber. After 2-day culture, MTEC/Plus with Tgfb inhibitor (SB431542, 10μM) (Sigma-Aldrich, 616461) or Tgfb1/2/3 ligands (10ng/ml, each) (R&D systems, 240-B/302-B2/243-B3) was placed in the upper and lower chambers. After 1-day culture, the cells on the Transwell insert were soaked in 400μl TRIzol™ Reagent (Invitrogen, 15596018) for Quantitative RT-PCR.

Ex-vivo trachea culture experiment

The developing tracheas dissected from E12.5 embryos were transferred onto the Whatman Nuclepore™ track-etched polycarbonate membrane (Whatman, 110614) and cultured at an air-liquid interface with DMEM/Ham's F-12 medium (Nacalai, 11582-05) supplemented with penicillin/streptomycin (Nacalai, 09367-34) and 5% FBS. The medium was changed every day in all experiments. The day when the ex-vivo trachea

146 culture experiment started was defined as day0. 10μM Y-27632 (LC laboratories, Y-5301)
147 was supplemented at Day0 and Day1 in all experiments. To assess the effects of cell cycle
148 status on the proliferation and differentiation processes in the tracheal epithelium, E12.5
149 trachea was cultured in the medium supplemented with or without PD00332991 (300nM,
150 600nM, or 900nM) (Abcam, 09367-34). At Day2, the cultured trachea was transferred
151 into 4% PFA for 30 min at 37 °C for fixation followed by PBS wash and the overnight
152 incubation in 30% sucrose at 4℃, and then embedded in OCT compound. To assess the
153 effects of Tgfb signaling on the proliferation and differentiation processes in the tracheal
154 epithelium, E12.5 trachea was cultured in the various conditions such as Tgfb inhibitor
155 treatment (SB431542, 2μM) (Sigma-Aldrich, 616461) and the combination treatment of
156 Tgfb1/2/3 ligands (10ng/ml, each) (R&D systems, 240-B/302-B2/243-B3). At Day2,
157 samples were collected and embedded in OCT compound in the same way described
158 above.

159 **Microscopy and imaging**

160 Tissue section immunofluorescence staining was imaged with LSM 710 confocal
161 microscopy (Carl Zeiss). Cells were counted based on nuclear staining with DAPI
162 (Nacalai, 11034-56) and specific cell markers of the respective cell types. Cells were
163 counted in the ventral region of trachea epithelium using ×63/1.4 NA Oil objective.

The tracheosphere was imaged using DP73 inverted microscopy (Olympus). Optical section images (512 x 512 to 800 x 800 pixels for the X-Y plane and 100μm for Z-axis step; 25-35 sections) was taken to estimate CFEs. Image processing and analyses were performed using ImageJ (NIH), ZEN2012 (Carl Zeiss), CellSens Dimension 2.1(Olympus), and Adobe Illustrator (Adobe).

Immunohistochemistry

For paraffin sections, dissected tracheas were dehydrated and embedded in paraffin. For frozen sections, dissected tracheas were incubation in 30% sucrose at 4˚C overnight, and then embedded in OCT compound. 6μm paraffin and 9μm frozen sections were used for immunohistochemistory experiments. The sections were treated for epitope retrieval with HistVT One (Nacalai, 06380) at 90 °C for 5 min or 105˚C for 15 min, permeabilized with 0.05% Tween in PBS, blocked using M.O.M. Immunodetection Kit (Vector laboratories, VEC-BMK-2202-1) for 1 hour at room temperature, then sections were incubated with primary antibodies at 4 ˚C for overnight. Detailed procedure and antibodies of each staining were listed below.

Antibody, Dilution	Company, Catalog code	Fixative	Tissue preparation	Antigen retrieval	Secondary antibody
GFP (1:400)	Thermo Fisher Scientific	4% PFA	Frozen	90°C, 5 min in Histo^{VT} One	Chicken Alexa488
GFP (1:500)	MBL international	4% PFA	Frozen	90°C, 5 min in Histo^{VT} One	Rabbit Alexa488
Scgb1a1	Santa Cruz	4% PFA	Paraffin	105°C, 15 min in Histo^{VT} One	Goat Alexa594

(1:500)					
Foxj1 (1:200)	eBioscience	4% PFA	Paraffin	105°C, 15 min in Histo^{VT} One	Mouse Alexa594
Ki67 (1:200)	BD Biosciences	4% PFA	Paraffin	105°C, 15 min in Histo^{VT} One	Mouse Alexa594
Krt17 (1:400)	Santa Cruz	4% PFA	Paraffin	105°C, 15 min in Histo^{VT} One	Mouse Alexa488
Krt17 (1:1000)	Abcam	4% PFA	Paraffin	105°C, 15 min in Histo^{VT} One	Rabbit Alexa488
Krt5 (1:1000)	Abcam	4% PFA	Paraffin	105°C, 15 min in Histo^{VT} One	Rabbit Alexa488
pSmad2/3 (1:200)	Cell Signaling	4% PFA	Frozen	90°C, 5 min in Histo^{VT} One	Rabbit Alexa488
Scgb3a2 (1:1000)	Dr. Shioko Kimura's lab	4% PFA	Paraffin	105°C, 15 min in Histo^{VT} One	Rabbit Alexa594
BrdU rat (1:100).	Abcam	4% PFA	Paraffin	105°C, 15 min in Histo^{VT} One	Rat Alexa488
p63 (1:1000)	Abcam	4% PFA	Paraffin	105°C, 15 min in Histo^{VT} One	Mouse Alexa647

After washing the slides with 0.05% Tween in PBS for 3 times, the sections were incubated with secondary antibodies for 1 hour at room temperature. All of secondary antibody conjugated with Alexa Fluor 488/594/647 (Life Technology) were used at 1:500 dilutions. Nuclei were stained with DAPI (Nacalai, 11034-56). The sections were mounted with Fluoromount™ (Diagnostic Biosystems, K024).

For the detection of pSmad2/3, Can Get Signal ® immunostain Solution B (Toyobo life science, NKB-601) was used as the solution for blocking buffer and primary/secondary antibodies.

Quantitative RT-PCR (qPCR)

Cells isolated by FACS were centrifuged and pelleted at 400*g* for 6min, then soaked in 400µl TRIzol™ Reagent (Invitrogen, 15596018). Total RNA was isolated with Direct-

zol RNA MicroPrep (Zymoresearch, R2060) according to the manufacturer's instructions. Reverse transcription reactions were performed with SuperScript™ III Reverse Transcriptase (Invitrogen, 18080) according to the manufacturer's instructions. qRT-PCR was performed on 7500 Real-Time PCR instrument (Applied Biosystems) using THUNDERBIRD® SYBR qPCR Mix (Toyobo life science, QPS-201). The mRNA levels of target genes were normalized to the Gapdh mRNA level. Primers used for qPCR are listed in KEY RESOURCES TABLE.

Single cell RNA-seq for sequencing library construction

To prepare single-cell suspensions of epithelial cells in 6 time points (E12.5, E13.5, E14.5, E16.5, and E18.5), the epithelial sheet was peeled off from mesenchymal tissue in developing trachea with a tungsten needle after the incubation with 175U/ml collagenase type Ⅰ (Worthington Biochemical Corporation, CLS1) at 37℃ for 6 - 60 min. Single-cell suspensions were made through the incubation with Trypsin-EDTA (0.25%) (Thermo Fisher Scientific, 25200056) at 37℃ for 15 min, then loaded onto Chromium Single Cell A Chips (10X Genomics, PN-1000009) for the Chromium Single Cell 3′ Library v2 (10X Genomics, PN-120233) according to the manufacturer's recommendations (10X Genomics). Briefly, single-cell gel bead-in-emulsions (GEMs) were generated from loaded cell suspensions by a Chromium Controller instrument (10X Genomics). After

208 performing GEM-reverse transcriptions (GEM-RTs), GEMs were harvested and the
209 cDNAs were amplified and cleaned up with SPRIselect Reagent Kit (Beckman Coulter,
210 B23318). Indexed sequencing libraries were constructed using Chromium Single Cell 3′
211 Library v2 (10X Genomics, PN-120233) for enzymatic fragmentation, end-repair, A-
212 tailing, adaptor ligation, ligation cleanup, sample index PCR, and PCR cleanup. Libraries
213 were sequenced on a HiSeq1500 (Illumina) to obtain a sequencing depth of around 50,000
214 reads per cells.

215 **Single cell RNA-seq Analysis**

216 The packages listed below was used for processing raw sequencing data and
217 downstream analysis; Cell Ranger version v2.2.0 (10X Genomics), Seurat version
218 v2.3.4(Butler, et al., 2018), and Monocle v2.8.0(Qiu, et al., 2017a; Qiu, et al., 2017b;
219 Trapnell, et al., 2014). First, the cells meeting any of the following criteria were omitted
220 from further analyses for the quality control; <1,000 or >5,000 UMIs, > 7.5% of reads
221 mapping to mitochondria genes, or EpCAM negative cells. For clustering, principal-
222 component analysis was performed for dimension reduction. Top 15 principal
223 components (PCs) were selected by using a permutation-based test implemented in
224 Seurat and passed to t-Distributed Stochastic Neighbor Embedding (tSNE) for
225 clustering visualization. To maintain a standard procedure for clustering, a value of 0.8

for the resolution was used. For the clustering analysis based on the expression of transcriptional factors, the gene list of mouse 1385 transcriptional factors derived from FANTOM5 SSTAR dataset (https://fantom.gsc.riken.jp/5/sstar/Browse_Transcription_Factors_mm9) (Lizio, et al., 2015) was used. Top 15 PCs and a value of 0.8 for the resolution were used for further clustering.

To delineate the developmental trajectories of lung progenitors in trachea, the Monocle2 algorithm (Qiu, et al., 2017a; Qiu, et al., 2017b; Trapnell, et al., 2014) was applied to the single cell dataset. Genes to be used for dimension reduction and ordering of the cells were determined by using the differentialGeneTest function in Monocle. The genes with a q-value < 0.01 were selected, and then sorted by q-value. The ordering gene set was used to compute a pseudotime graph by using the reduceDimension function (using the DDRTree method), followed by the orderCells function. To estimate the comprehensive linage map of the epithelial progenitors (Figure 1C), the unsupervised analysis was conducted without any specific cell markers. To estimate the developmental trajectories of Krt17+ and Krt17- progenitors (Figure 1H and 1I), first, the cells in S and G2-M phases were omitted. Then, the semi-supervised analysis was conducted based on Krt17 expression.

244 **Single molecule in-situ hybridization (PLISH)**

245 Single molecule in situ hybridization of mRNAs called PLISH (Proximity Ligation In
246 Situ Hybridization) was performed by following the procedures described in the past
247 paper (Nagendran, et al., 2018). Briefly, OCT-embedded, frozen 9μm tissue sections are
248 used to hybridize with anti-sense probe pairs that anneal at adjacent positions in a tiled
249 manner along a target transcript. After the subsequent addition of circle and bridge
250 oligonucleotides (circle components) harboring a specific 'barcode' sequence, the nicks
251 in the junction were sealed by ligation with T4 DNA Ligase (New England BioLabs,
252 M0202T) to create a covalently closed circle. Using the circularized probes as a template,
253 complementary tandem repeats were generated through rolling-circle amplification
254 (RCA) with NxGen® phi29 DNA Polymerase (Lucigen, 30221). The single-stranded
255 amplicons were detected with a Cy5-labeled oligonucleotide (Cy5-DP5) that is
256 complementary to the specific 'barcode'. The sets of probe pairs, circle components, and
257 Cy5-labele oligonucleotide used to detect transcripts of the indicated genes are listed in
258 KEY RESOURCES TABLE.

259 **Single molecule in-situ hybridization (RNAscope)**

260 Single molecule in situ hybridization of mRNAs called RNAscope was performed by

following the manufacturer's instructions. Briefly, OCT-embedded, frozen 9μm tissue sections are used to hybridize with the proprietary probes for *Id2* RNA using RNAscope Multiplex Fluorescent Reagent Kit v2 (Advanced Cell Diagnostics).

SO_2 airway injury model

SO_2 injury models have been previously described (Pardo-Saganta, et al., 2015; Rawlins, et al., 2007; Borthwick, et al., 2001). Briefly, 8-16 weeks old male mice were exposed to 700 ppm SO_2 for 4 hours. Age-matched mice were used for both control and mutant mice (Shh^{Cre}, $Rosa^{3xHA\text{-}Id2\text{-}IRES\text{-}H2B\text{-}EGFP}$ mice; Id2 OE or Shh^{Cre}, $Tgfbr2^{flox/flox}$ mice; Tgfbr2 cKO). Mouse tracheas were collected 12, 18, 24, 48, 72, and 120 hours after injury. 3-4 tracheas at each time point were analyzed.

STATISTICAL ANALYSIS

Statistical analyses were performed with Microsoft Excel for Mac. For paired comparisons, statistical significance was determined by Student's t-test. For multiple comparisons, statistical significance was determined by Tukey's method.

DATA AND CORE AVAILABILITY

The scRNA-seq datasets in this paper is accessible at GSE152692. Token is itulegeoxtkzxet. (https://www.ncbi.nlm.nih.gov/geo/query/acc.cgi?acc=GSE152692)

References

Abe, T., Inoue, K.I., Furuta, Y., and Kiyonari, H. (2020). Pronuclear Microinjection during S-Phase Increases the Efficiency of CRISPR-Cas9-Assisted Knockin of Large DNA Donors in Mouse Zygotes. Cell Rep 31, 107653.

Abe, T., Sakaue-Sawano, A., Kiyonari, H., Shioi, G., Inoue, K., Horiuchi, T., Nakao, K., Miyawaki, A., Aizawa, S., and Fujimori, T. (2013). Visualization of cell cycle in mouse embryos with Fucci2 reporter directed by Rosa26 promoter. Development 140, 237-46.

Borthwick, D.W., Shahbazian, M., Krantz, Q.T., Dorin, J.R., and Randell, S.H. (2001). Evidence for stem-cell niches in the tracheal epithelium. Am J Respir Cell Mol Biol 24, 662-70.

Butler, A., Hoffman, P., Smibert, P., Papalexi, E., and Satija, R. (2018). Integrating single-cell transcriptomic data across different conditions, technologies, and species. Nat Biotechnol 36, 411-420.

Lizio, M., Harshbarger, J., Shimoji, H., Severin, J., Kasukawa, T., Sahin, S., Abugessaisa, I., Fukuda, S., Hori, F., Ishikawa-Kato, S., et al. (2015). Gateways to the FANTOM5 promoter level mammalian expression atlas. Genome Biol 16, 22.

Nagendran, M., Riordan, D.P., Harbury, P.B., and Desai, T.J. (2018). Automated cell-type classification in intact tissues by single-cell molecular profiling. Elife 7.

Niwa, H., Yamamura, K., and Miyazaki, J. (1991). Efficient selection for high-expression transfectants with a novel eukaryotic vector. Gene 108, 193-9.

Pardo-Saganta, A., Law, B.M., Tata, P.R., Villoria, J., Saez, B., Mou, H., Zhao, R., and Rajagopal, J. (2015). Injury induces direct lineage segregation of functionally distinct airway basal stem/progenitor cell subpopulations. Cell Stem Cell 16, 184-97.

Qiu, X., Hill, A., Packer, J., Lin, D., Ma, Y.A., and Trapnell, C. (2017a). Single-cell mRNA quantification and differential analysis with Census. Nat Methods 14, 309-315.

Qiu, X., Mao, Q., Tang, Y., Wang, L., Chawla, R., Pliner, H.A., and Trapnell, C. (2017b). Reversed graph embedding resolves complex single-cell trajectories. Nat Methods 14, 979-982.

Rawlins, E.L., Ostrowski, L.E., Randell, S.H., and Hogan, B.L. (2007). Lung development and repair: contribution of the ciliated lineage. Proc Natl Acad Sci U S A 104, 410-7.

Srinivas, S., Watanabe, T., Lin, C.S., William, C.M., Tanabe, Y., Jessell, T.M., and Costantini, F. (2001). Cre reporter strains produced by targeted insertion of EYFP and ECFP into the ROSA26 locus. BMC Dev Biol 1, 4.

Trapnell, C., Cacchiarelli, D., Grimsby, J., Pokharel, P., Li, S., Morse, M., Lennon, N.J., Livak, K.J., Mikkelsen, T.S., and Rinn, J.L. (2014). The dynamics and regulators of cell fate decisions are revealed by pseudotemporal ordering of single cells. Nat Biotechnol 32, 381-386.